RESEARCH ARTICLE SUMMARY

IMMUNOLOGY

Sexual dimorphism in skin immunity is mediated by an androgen-ILC2-dendritic cell axis

Liang Chi*, Can Liu†, Inta Gribonika, Julia Gschwend, Dan Corral, Seong-Ji Han, Ai Ing Lim, Claudia A. Rivera, Verena M. Link, Alexandria C. Wells, Nicolas Bouladoux, Nicholas Collins, Djalma S. Lima-Junior, Michel Enamorado, Barbara Rehermann, Sophie Laffont, Jean-Charles Guéry, Roxane Tussiwand, Christoph Schneider, Yasmine Belkaid*

INTRODUCTION: Sexual dimorphisms have been observed in the susceptibility to many cancers, autoimmune disorders, and infectious diseases such as COVID-19. Differences in the immune system between females and males is thought to contribute to the observed sex-related bias in disease outcomes. Barrier tissues are a primary target of infections and injury. In addition, these sites are continuously colonized by a complex microbial community that also regulates host defense. However, sex-related immune differences in barrier tissues, and how these may be shaped by microbiota, are poorly understood. Expanding the current knowledge about sexual dimorphisms of the immune system may provide insights toward developing sex-refined therapeutic strategies for many diseases.

RATIONALE: We used mice as a model system with which to compare the innate and adaptive immune cell subsets present in barrier tissues between females and males and to investigate how immunity may underpin sexual dimorphisms in disease outcome.

RESULTS: Adult female mice had a higher level of skin-resident T cells than did males. These sex-related differences were tissue specific, because we did not observe sex-related differences in the composition of immune cells in the small intestine or in ear-draining lymph nodes. The sex-associated differences in T cell composition in the skin were observed in germ-free mice, which lack microbiota. However, reintroducing a skin microbiome into these mice augmented sex differences in females. We also observed that females had a higher magnitude of skin adaptive immune responses than did males in response to new commensals (*Staphylococcus epidermidis*, *Corynebacterium accolens*, or *Candida albicans*) colonizing the skin or skin infection with *S. aureus*. Sex differences in the composition of the skin immune system were not observed in mice that had not reached adulthood. In addition, castration of male mice before sexual maturation normalized the skin immune cell numbers and the potency of adaptive immune responses to microbiota to the level seen in females, suggesting a key role for male sex hormones in shaping sex-related differences in skin immunity.

In addition to T cells, we observed a higher level of skin-resident dendritic cell subsets (DCs) in females than males, including type 1 conventional DCs (cDC1s), Langerhans cells (LCs), and CD11b^{low} type 2 conventional DCs (cDC2s). DCs play a fundamental role in antigen presentation and triggering of adaptive immune responses. Single-cell RNA sequencing (scRNA-seq) revealed that skin DCs from females had a more activated gene expression signature than did DCs from males. Functional evaluation of DCs confirmed that DCs from the skin of female mice had enhanced migratory and T cell–priming capabilities compared with those from males. Sex-related differences of skin DCs were dependent on male sex hormones, because castration increased the level of those DCs in males, and testosterone injection decreased skin DC levels in females.

The androgen receptor (AR) was not expressed by skin DCs, suggesting that androgens regulate DCs indirectly. Type 2 innate lymphoid cells (ILC2s) are abundant in the skin and, based on scRNA-seq data, express a higher level of AR than other skin lymphocytes. Female mice had a higher number of skin ILC2s, with a more activating gene expression signature, and produced a higher level of cytokines than ILC2s from males. These differences could be abrogated in male mice by castration or AR knockout.

ILC2-deficient transgenic mice (*Rag2*$^{-/-}\gamma c^{-/-}$ mice) had a disrupted skin DC network, characterized by a decrease of skin cDC1s, LCs, and CD11b^{low} cDC2s. Adoptive transfer of skin ILC2s to *Rag2*$^{-/-}\gamma c^{-/-}$ mice rescued the level of skin cDC1s. By using a granulocyte-macrophage colony-stimulating factor (GM-CSF) reporter mouse, we found that most skin ILC2s produced GM-CSF, which is a key cytokine for maintaining the survival of dermal cDC1s. Correspondingly, transferring ILC2s deficient in GM-CSF production (*Csf2*$^{-/-}$ ILC2s) did not restore the skin cDC1 population, supporting the idea that ILC2s maintain skin cDC1 through the production of GM-CSF.

CONCLUSION: Skin ILC2s are master players helping to maintain skin DC network homeostasis by producing essential cytokines. Male sex hormones, by negatively regulating skin ILC2s, lead to differences in the DC network, resulting in a heightened adaptive immune response in female mice compared with male mice during commensal colonization and infection. ■

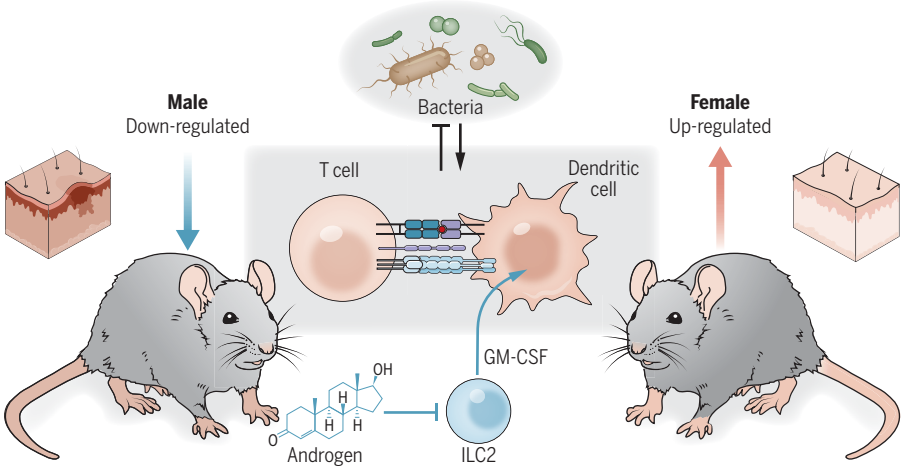

ILLUSTRATION: N. CARY/*SCIENCE* BASED ON LIANG CHI

Male sex hormones down-regulate skin immunity in male mice by negatively regulating the ILC2-DC axis. ILC2s produce cytokines that maintain skin DC levels. Androgens, acting through the AR, negatively regulate skin ILC2s, causing sex-related differences in ILC2 and downstream DC populations, which may then affect T cell responses. Therefore, androgen effects on the skin ILC2-DC axis may contribute to the sex bias of adaptive immune responses to bacterial colonization and infection.

The list of author affiliations is available in the full article online.
*Corresponding author. Email: ybelkaid@niaid.nih.gov (Y.B.); liang.chi@nih.gov (L.C.)
†Present address: Department of Immunobiology, Yale University School of Medicine, New Haven, CT 06510, USA
Cite this article as L. Chi *et al.*, *Science* **384**, eadk6200 (2024). DOI: 10.1126/science.eadk6200

READ THE FULL ARTICLE AT
https://doi.org/10.1126/science.adk6200

RESEARCH ARTICLE

IMMUNOLOGY

Sexual dimorphism in skin immunity is mediated by an androgen-ILC2-dendritic cell axis

Liang Chi[1]*, Can Liu[2]†, Inta Gribonika[1], Julia Gschwend[3], Dan Corral[1], Seong-Ji Han[1], Ai Ing Lim[1], Claudia A. Rivera[1], Verena M. Link[1], Alexandria C. Wells[1], Nicolas Bouladoux[1], Nicholas Collins[1], Djalma S. Lima-Junior[1], Michel Enamorado[1], Barbara Rehermann[4], Sophie Laffont[5], Jean-Charles Guéry[5], Roxane Tussiwand[6], Christoph Schneider[3], Yasmine Belkaid[1,7]*

Males and females exhibit profound differences in immune responses and disease susceptibility. However, the factors responsible for sex differences in tissue immunity remain poorly understood. Here, we uncovered a dominant role for type 2 innate lymphoid cells (ILC2s) in shaping sexual immune dimorphism within the skin. Mechanistically, negative regulation of ILC2s by androgens leads to a reduction in dendritic cell accumulation and activation in males, along with reduced tissue immunity. Collectively, our results reveal a role for the androgen-ILC2-dendritic cell axis in controlling sexual immune dimorphism. Moreover, this work proposes that tissue immune set points are defined by the dual action of sex hormones and the microbiota, with sex hormones controlling the strength of local immunity and microbiota calibrating its tone.

The immune system serves as a potent rheostat of host physiology, a fundamental function that requires specialized regulation across tissues, age, and biological sex. Such tailored control also contributes to differences in disease manifestations. Sex bias in host immunity is believed to account for differences in the incidence, tropism, and severity of diseases between males and females. Clinical and experimental work revealed that females tend to develop stronger responses to infections and vaccines and have a greater incidence of autoimmune disorders than males (*1*). As an illustration of this phenomenon, sex differences in infection outcomes were recently highlighted in the context of the severe acute respiratory syndrome coronavirus 2 (SARS-CoV-2) pandemic, with enhanced risk for severe infection and lethality found in men compared with women (*2*). Differential susceptibility to infections and inflammatory disorders has been, at least in part, attributed to heightened innate and adaptive immune potency in females compared with males (*3*, *4*). Although several mechanisms have been proposed to account for this phenomenon, our understanding of the key players involved in shaping sex-specific immunity remains sparse.

Sexual dimorphism can result from sex chromosome and/or hormonal control of host physiology (*1*). Both androgens and estrogens have been shown to have the capacity to directly affect the function of various immune cells (*1*). For example, the direct action of estrogen on $CD4^+$ T cells can contribute to the development of T cell–dependent autoimmune inflammation (*5*). The androgen receptor (AR) has been shown to be expressed in several cell subsets, including type 2 innate lymphoid cells (ILC2s), macrophages, and $CD8^+$ T cells, and signaling through this pathway is generally considered to be immunosuppressive (*6*). Recent studies have demonstrated that AR signaling was able to suppress $CD8^+$ T cell–dependent antitumor immunity through negative regulation of T cell differentiation (*7*–*9*).

Sexual bias in host immunity is of particular importance in barrier tissues that are the primary targets of infections, injury, and chronic inflammatory disorders (*10*). Indeed, sexual dimorphism has long been recognized to be involved in various barrier tissue inflammatory disorders such as asthma, atopic dermatitis, and Sjögren's syndrome (*11*, *12*). Collectively, biological sex has broadly been associated with differences in the intensity and tropism of numerous disorders. How constitutive wiring of barrier tissues in males versus females predicts disease outcomes remains largely unclear, but emerging evidence supports the idea that each tissue may be differentially affected by biological sex. For instance, comparison of 44 human tissues revealed tissue-specific differences in the number of genes differentially regulated between men and women, with the skin notably displaying the highest number of sex-biased genes (*13*).

Host physiology is also dominantly shaped by the microbiota, which, through its ability to act as a major physiological stressor, controls tissue development, immunity, and repair (*14*, *15*). Although previous work has uncovered differences in microbiota composition between males and females (*16*), how responses to the microbiota are shaped by sexual differences and whether this in turn allows the microbiota to further calibrate its physiological impact on host immunity have not been addressed. Moving forward, determining what drives and sustains sexual immune dimorphism, including in the context of environmental stressors, will be important for understanding health and disease.

Here, we aimed to identify key factors involved in the control of tissue-specific immune sexual bias. Our work uncovers a dominant role for ILC control of tissue-resident dendritic cells (DCs) in shaping sexual immune differences in the skin, with sex hormones mediating the strength of local immunity and the microbiota calibrating its tone.

Females have a higher accumulation of T cells in the skin at steady state and in response to the microbiota than do males

To uncover the determinants of sex-biased immunity in barrier tissues, we profiled the lymphoid landscape of three major barrier sites, skin, lung, and gut, from sexually mature male and female mice. Consistent with previous reports of heightened immunity in females (*1*), we found that at steady state, the number of major classical T cell subsets [type 17 T helper (Th17) cells, Th1 cells, type 17 cytotoxic T (Tc17) cells, Tc1 cells, as well as $GATA3^+$ and $ROR\gamma t^+$ regulatory T (T_{reg}) cells] was higher in the skin and lung of females compared with males (Fig. 1A and fig. S1A). Conversely, no difference was detected within the skin-draining lymph nodes (fig. S1B) nor within the small intestine (Fig. 1A). Thus, at steady state, immune sex bias may be dominantly imposed within defined tissues and/or compartments.

To investigate whether immune sex differences are microbiota dependent, we assessed T cell phenotypes and numbers within tissues of female and male germ-free mice. Sex differences in T cells were observed in the skin of germ-free mice, but were not detected within the lung, supporting the idea that the skin was affected by sex in a microbiota-independent manner (Fig. 1B). This observation, coupled with the fact that in humans defined gene expression

[1]Metaorganism Immunity Section, Laboratory of Host Immunity and Microbiome, National Institute of Allergy and Infectious Diseases, National Institutes of Health, Bethesda, MD 20892, USA. [2]Multiscale Systems Biology Section, Laboratory of Immune System Biology, National Institute of Allergy and Infectious Diseases, National Institutes of Health, Bethesda, MD 20892, USA. [3]Institute of Physiology, University of Zurich, CH-8057 Zürich, Switzerland. [4]Immunology Section, Liver Diseases Branch, National Institute of Diabetes and Digestive and Kidney Diseases, National Institutes of Health, Bethesda, MD 20892, USA. [5]Toulouse Institute for Infectious and Inflammatory Diseases (Infinity), INSERM UMR1291, CNRS UMR5051, University Toulouse III, Toulouse, France. [6]National Institute of Dental and Craniofacial Research, National Institutes of Health, Bethesda, MD 20892, USA. [7]NIAID Microbiome Program, National Institute of Allergy and Infectious Diseases, National Institutes of Health, Bethesda, MD 20892, USA.
*Corresponding author. Email: ybelkaid@niaid.nih.gov (Y.B.); liang.chi@nih.gov (L.C.)
†Present address: Department of Immunobiology, Yale University School of Medicine, New Haven, CT 06510, USA.

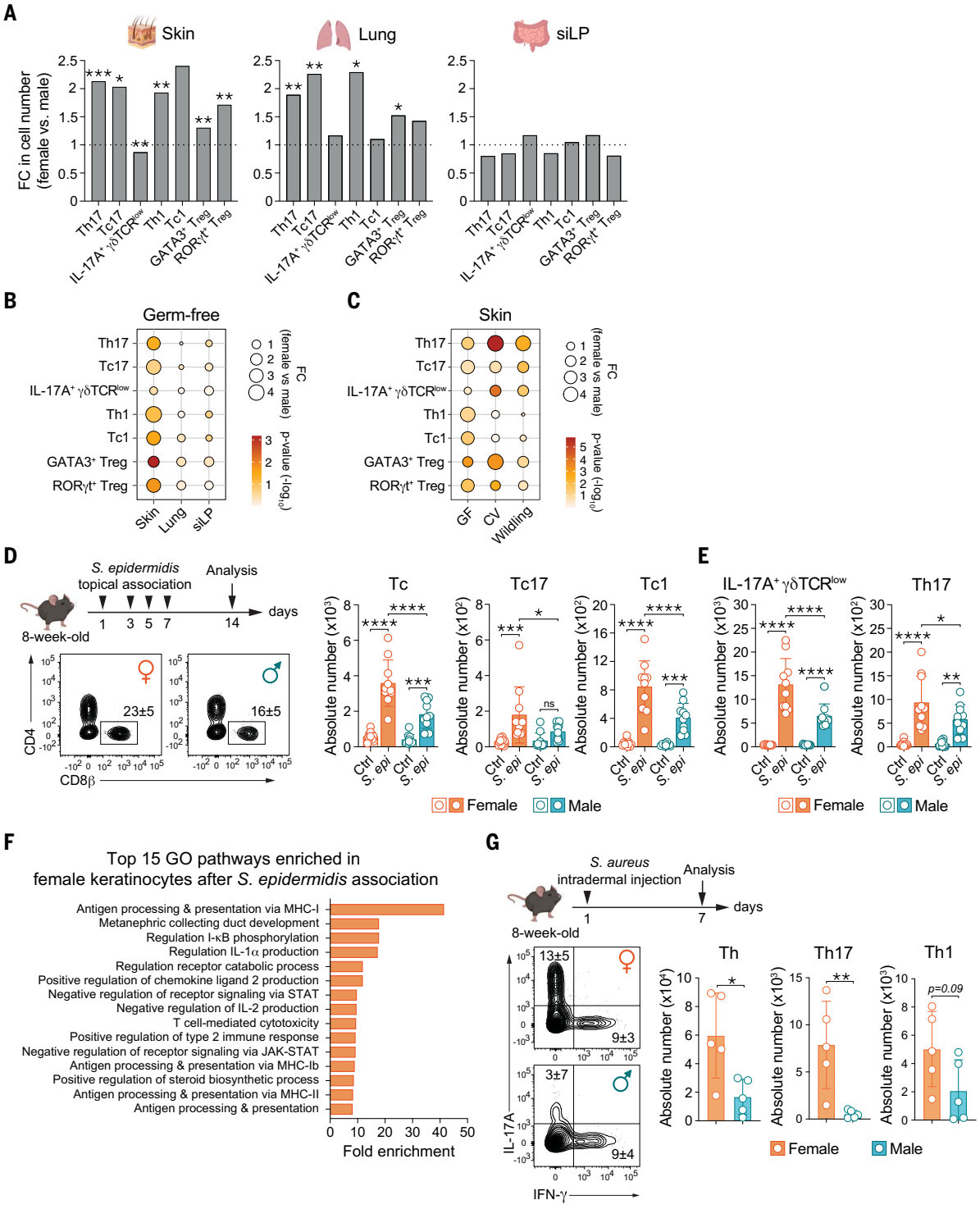

Fig. 1. Females have higher T cell accumulation in the skin at steady state and in response to the microbiota and pathogen. (**A**) Fold changes in absolute numbers of various lymphocyte cell populations, including Th17, Tc17, IL-17A$^+$ γδTCR^{low}, Th1, Tc1, GATA3$^+$ T_{reg}, and RORγt$^+$ T_{reg} cells, in the ear skin, lung, and small intestine of female adult mice compared with males. (**B**) Fold changes in absolute numbers (represented by the size of the circles) and *P* value (represented by the color of the circles) of lymphocyte subsets in various tissues of germ-free female mice compared with males. (**C**) Fold changes in absolute numbers (represented by the size of the circles) and *P* value (represented by the color of the circles) of lymphocyte subsets in the skin of germ-free mice (GF), conventionalized germ-free mice (CV), and wildling mice. (**D** to **F**) Adult females and males were topically associated with *S. epidermidis* (*S. epi*) or left unassociated (Ctrl). (D) Left: representative contour plots showing frequencies of CD8β$^+$ T cells (gating at live CD45$^+$ CD90.2$^+$ TCRβ$^+$ Foxp3$^-$) in *S. epidermidis*–associated females and males. Right: bar graphs showing the absolute numbers of total Tc cells, Tc17 cells, and Tc1 cells per ear pinnae in unassociated and *S. epidermidis*–associated female and male mice. (E) Bar graphs showing the absolute numbers of IL-17A$^+$ γδTCR^{low} cells and Th17 cells in unassociated and *S. epidermidis*–associated female and male mice. (F) Bulk RNA-seq of keratinocytes sorted from the skin of *S. epidermidis*–associated female and male mice. Bar graph represents the top 15 pathways by GO enrichment analysis enriched in

keratinocytes from *S. epidermidis*–associated females compared with *S. epidermidis*–associated males. (**G**) Representative contour plots (left) showing frequencies of live CD45$^+$ CD90.2$^+$ TCRβ$^+$ Foxp3$^-$ Th17 or Th1 CD4$^+$ T cells in female and male mice infected intradermally with *S. aureus*. Bar graphs (right) show absolute numbers per ear pinnae of Th, Th17, and Th1 cells in *S. aureus*–infected female and male mice. For (A) to (E) and (G), data are representative of at least two independent experiments. Each dot represents an individual mouse: for (A), n = 10 to 40 mice per sex; for (D) and (E), n = 10 mice per sex; and for (B), (C), (F), and (G), n = 5 to 8 mice per sex. Numbers in representative flow plots indicate mean ± SD. *P < 0.05; **P < 0.01; ***P < 0.001; ****P < 0.0001; ns, not significant. For (A) to (C) and (G), two-tailed unpaired Student's t test was used and for (D) and (E), two-way ANOVA was used. See also fig. S1.

in the skin is affected the most by sex differences (*13*), led us to subsequently focus on this compartment.

Although the microbiota was not required to impose differences in the skin between males and females, we assessed whether it could further shape immune bias. Introduction of a complex microbiota (conventionalization) to adult germ-free mice further amplified sex differences between males and females and, more specifically, those differences linked to type 17 and T$_{reg}$ cell responses, supporting the idea that the microbiota can shape sex bias toward type 17 and T$_{reg}$ cell immunity in females (Fig. 1C). We next investigated whether differences between males and females in skin immunity were also observed in wildling mice, those born with natural, wild-derived microbiota and pathogens (*17*). These mice also displayed a strong sex bias, particularly heightened type 17 cell responses, in females compared with males (Fig. 1C).

We previously showed that skin colonization with a new commensal was associated with the accumulation of interleukin-17A (IL-17A)–producing T cells within the skin (*18*–*21*). These responses occur in a manner uncoupled from inflammation and provide long-term benefits to the host, including enhanced protection against infections and accelerated wound healing (*18*–*20*). We next assessed whether responses to *Staphylococcus epidermidis* are also shaped by biological sex. After topical association with *S. epidermidis*, a process that we have previously shown to allow microbial colonization (*18*–*22*), the level of IL-17A– and interferon-γ–(IFN-γ)–producing CD8$^+$ T cells (Tc17 and Tc1 cells, respectively) and other dominant IL-17A–expressing immune cells (IL-17A$^+$ γδTCR^{low} and Th17) accumulating within the skin were higher in females compared with males (Fig. 1, D and E). Conversely, no difference was detected in the numbers of dendritic epidermal T cells (γδTCR^{high}) at steady state, and we observed a moderate decrease in males compared with females after *S. epidermidis* association (fig. S1C). T cell responses to skin microbes can affect keratinocyte homeostasis and barrier function (*18*, *22*); therefore, we compared keratinocyte responses to *S. epidermidis* association between males and females by bulk RNA sequencing (RNA-seq). Gene ontology (GO) enrichment analysis revealed that several immune-associated pathways were enriched in female keratinocytes compared with those from males. These included an increase in antigen processing and presentation pathways in females, a response that we previously showed to reinforce local commensal-induced T cell retention (*22*) (Fig. 1F). Pathways associated with IL-1α and chemokine production were also increased in female keratinocytes compared with males (Fig. 1F). Reduced barrier immunity in males compared with females was functionally highlighted by enhanced bacterial burden at the skin surface of males compared with females after *S. epidermidis* topical association (fig. S1D). We next compared responses of males and females to another skin commensal, *Corynebacterium accolens*, which we previously showed to promote the accumulation of IL-17A$^+$ γδTCR^{low} cells (*21*). Whereas the total number of γδTCR^{low} cells was comparable between males and females at steady state, females accumulated a higher number of IL-17A$^+$ γδTCR^{low} cells within the skin after *C. accolens* topical association than did males (fig. S1E). Similarly, skin T cell responses to *Candida albicans* associated as a commensal were higher in females than in males (fig. S1F). We next investigated whether differences in homeostatic immunity between males and females translated to infection. Mice were infected intradermally with *S. aureus*. At day 7 after infection, skin CD4$^+$ T helper cell (Th) responses, including Th1 and Th17, were lower in males compared with females (Fig. 1G). Thus, responses to the microbiota (both T cells and keratinocytes), as well as T cell responses to infection, are differentially affected by sex, with enhanced immune responses in females compared with males.

Sex immune differences within the skin are imposed by male sex hormones

Sex differences can result from hormonal and/or sex chromosome control of host physiology (*1*). Sex hormones are maintained at low levels until puberty, when their sharp increase contributes to sexual maturation (*23*). In the present study, differences in the lymphoid landscape between males and females were only detectable after sexual maturation, supporting the idea that sex hormones may play a dominant role in the phenotype observed (Fig. 2A). To further test this possibility, gonads were removed from male and female mice before sexual maturation, and T cell composition and phenotype were assessed in adult mice. Removal of ovaries from females had no effect on the skin lymphoid composition (Fig. 2B). By contrast, male castration restored the number and frequency of IL-17A–producing cells (Tc17 and Th17 cells), as well as T$_{reg}$ cells (expressing GATA3 or RORγt) to the levels observed in females (Fig. 2C and fig. S2A). Male castration also restored the ability of males to develop CD8$^+$ T cells (Tc17 and Tc1 cells) and IL-17A–producing γδT cells (IL-17A$^+$ γδTCR^{low} cells and Th17) in response to *S. epidermidis* in a manner comparable to females (Fig. 2, D and E, and fig. S2B). Consistent with heightened immunity resulting from castration, bacterial burden was decreased in castrated mice compared with sham controls (fig. S2C). These results support the idea that male sex hormones control sex lymphoid bias in the skin both at steady state and in response to the microbiota.

DC homeostasis is regulated by male sex hormones

DCs are the primary sensors and mediators of tissue immunity, and T cell responses to *S. epidermidis* are controlled by the cooperation among diverse subsets of tissue-resident DCs (*19*). Therefore, we next explored the possibility that lymphocyte differences between males and females could result from quantitative and/or functional differences in the skin DC network. At steady state, the skin contains several DC subsets, namely type 1 conventional DCs (XCR1$^+$ CD103$^+$ cDC1s), Langerhans cells (LCs), type 2 conventional DCs (CD11b^{hi} cDC2s), and the more recently described CD11b^{low} cDC2 subset (CD301b$^+$ DCs) (*24*, *25*) (Fig. 3A and fig. S3A). The overall composition of the DC network was broadly comparable between male and female mice. Conversely, the absolute number of all resident DC subsets (cDC1s, LCs, and CD11b^{low} cDC2s), with the exception of CD11b^{hi} DC2s, was higher in the skin of females compared with males (Fig. 3B).

To determine whether there were also qualitative differences between male and female DCs, we performed a droplet-based 3′ single-cell RNA-seq (scRNA-seq) of DCs from the skin of males and females. In agreement with flow cytometry analysis, the overall composition of the skin DC network was comparable between males and females (Fig. 3C). Conversely, the transcriptional profiles of DCs from males and females were distinct for each subset analyzed, with increased expression of genes associated with activation and differentiation in females compared with males (Fig. 3D). For instance, cDC1s isolated from female skin expressed a higher level of *Adam23*, the product of which promotes antigen presentation, and a higher level of genes encoding a kinase involved in

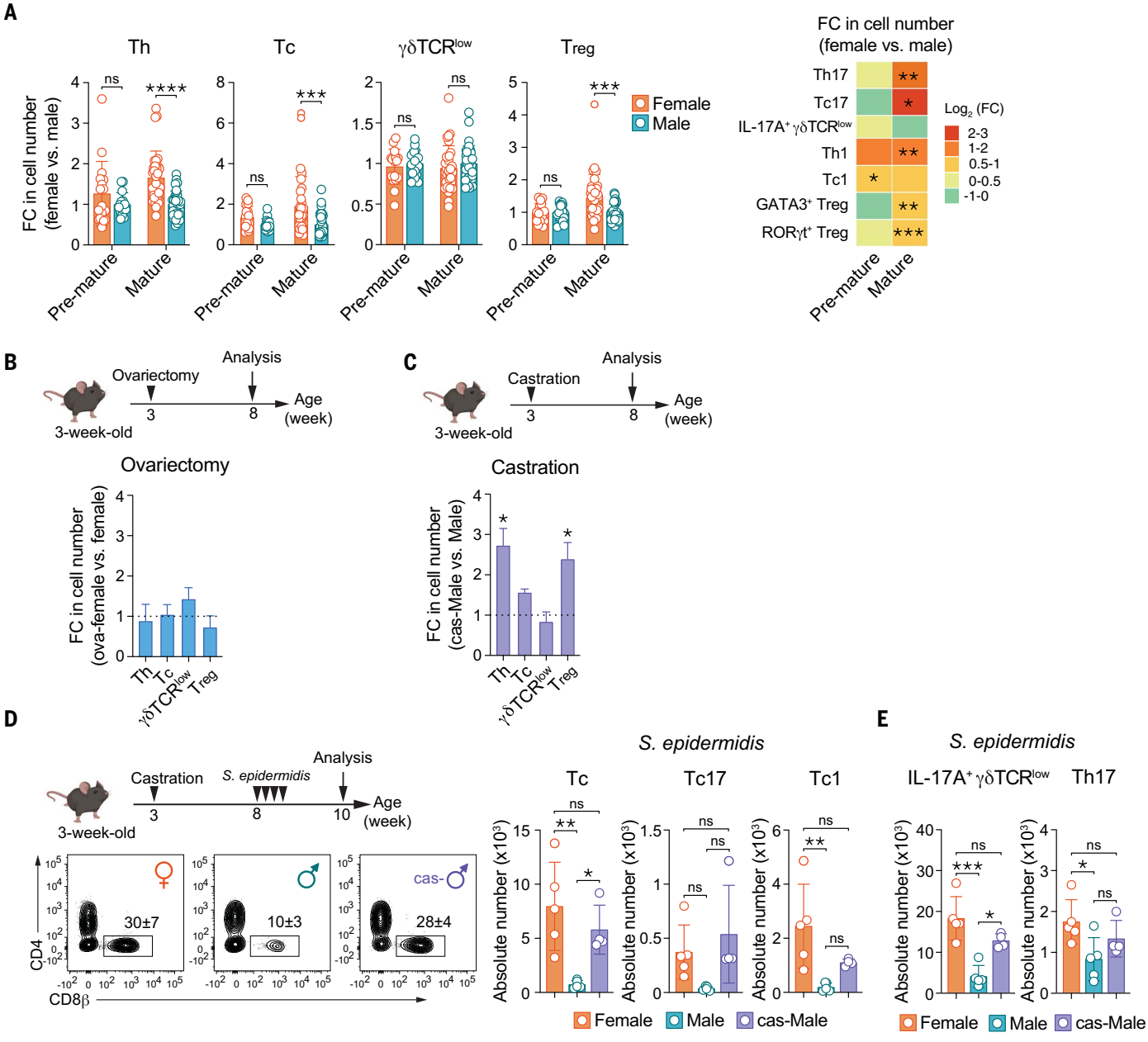

Fig. 2. Sex immune differences within the skin are imposed by sex hormones. (**A**) Fold changes in absolute numbers of lymphocyte subsets in the ear skin from 3- to 4-week-old (premature) mice and 8- to 10-week-old (mature) mice. (**B** and **C**) Three-week-old female and male mice were castrated or ovariectomized or had a sham surgery as control. Skin immune cells were analyzed at 8 weeks of age. Bar graphs show fold changes in absolute numbers of lymphocyte subsets in the skin of adult ovariectomized females (B) and adult castrated males (C) compared with adult control mice (sham surgery). (**D**) Three-week-old female and male mice were castrated or underwent sham surgery as a control. *S. epidermidis* association was performed at 8 weeks of age, and then immune reponses were analyzed at 10 weeks. Left: representative contour plots showing frequencies of CD8β$^+$ T cells (gating at live CD45$^+$ CD90.2$^+$ TCRβ$^+$ Foxp3$^-$) in adult females, males, and castrated males (cas-♂) topically associated with *S. epidermidis*. Right: bar graphs showing absolute numbers of total Tc, Tc17, and Tc1 cells in *S. epidermidis*–associated females, males, and castrated males (cas-Male). (**E**) Bar graphs showing absolute numbers of IL-17A$^+$ γδTCR^{low} cells and Th17 in *S. epidermidis*–associated female and male mice. Data are representative of at least two independent experiments. Each dot represents an individual mouse: for (A), n = 15 to 30 mice per sex; for (B) and (C), n = 3 mice per sex; for (D) and (E), n = 4 to 5 mice per sex. Numbers in representative flow plots indicate mean ± SD. *P < 0.05; **P < 0.01; ***P < 0.001; ****P < 0.0001; ns, not significant. For (A), two-way ANOVA was used; for (B) and (C), two-tailed unpaired Student's t test was used; and for (D) and (E), one-way ANOVA was used.

enhanced resistance to oxidative stress (*Oxsr1*) (*26*) and a T cell–attracting chemokine (*Ccl17*) (*27*). LCs isolated from female skin expressed a higher level of genes linked to costimulation and survival, such as *Cd40* and *Anxa1* (*28*, *29*). CD11b^{low} cDC2 from females similarly expressed a higher level of genes involved in costimulation (*Cd40*), DC maturation (*Cd83*), and antigen presentation (*Adam23*) (Fig. 3D). Female CD11b^{hi} cDC2s also expressed a higher level of genes associated with cDC2 development (*Irf4*), T cell–attracting chemokines (*Ccl17*),

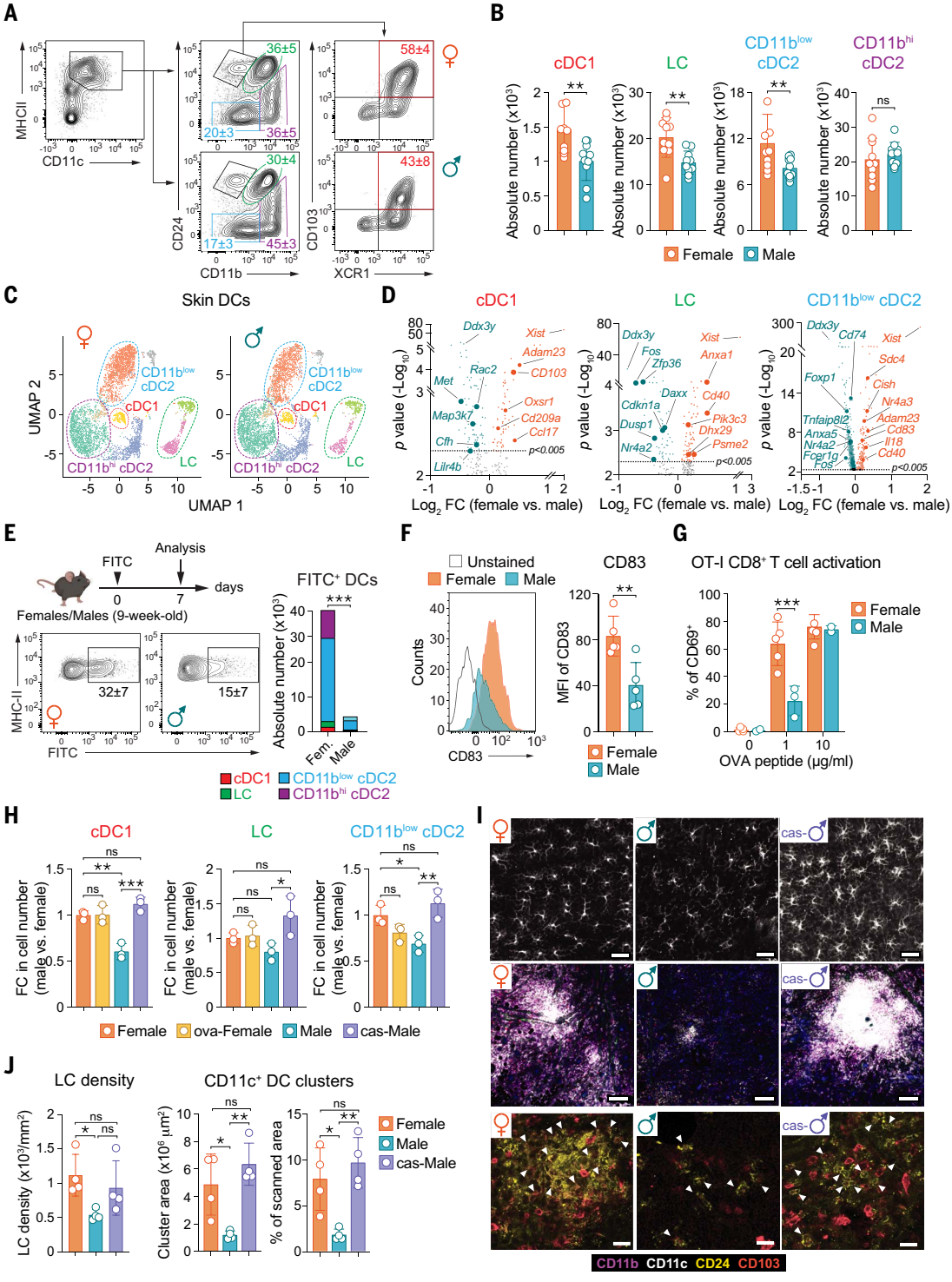

Fig. 3. DC homeostasis is regulated by sex hormones. (**A** to **D**) DC populations in the skin of adult female and male mice were analyzed by flow cytometry and scRNA-seq. (A) Representative contour plots of DC subsets within the skin of adult female and male mice. (B) Absolute numbers of DC subsets in adult female and male mice (see fig. S3A for gating strategy). (C) UMAP projection plots showing skin DC clusters analyzed by scRNA-seq (cell number: female, 5287; male, 5067). (D) Volcano plots displaying differentially expressed genes in cDC1s, LCs, and CD11b^{low} cDC2s between adult female and male mice. Highly expressed genes in females are shown in orange, and highly expressed genes in males are shown in teal. (**E**) Left: representative contour plots of FITC$^+$ DCs within the skin-draining lymph nodes of adult female and male mice 2 days after FITC application. Right: bar graph showing absolute numbers of FITC$^+$ DC subsets in adult female and male mice. (**F**) Left: histogram plot showing the expression level of CD83 in FITC$^+$ DCs. Right: bar graph showing the mean fluorescence intensity of CD83 in FITC$^+$ DCs in female and male mice. (**G**) Bar graph showing the frequencies of CD69$^+$ OVA-specific CD8$^+$ T cells after 18 hours of priming with skin OVA peptide-loaded cDC1s from female and male mice. (**H**) Fold change in absolute number of DC subsets in the skin of adult ovariectomized females (ova-Female), castrated males (cas-Male), and males (sham surgery) compared with females (sham surgery). (**I**) Top: representative

confocal images of whole-mount ear pinnae of females, males, and castrated males (cas-♂) stained for CD11c. Scale bars, 30 μm. Middle: representative confocal images of whole-mount ear pinnae from females, males, and castrated males showing dermal DC clusters stained for DAPI, CD11c, CD24, CD103, and CD11b. Scale bars, 200 μm. Bottom, representative confocal images of whole-mount ear pinnae from females, males, and castrated males showing cDC1s stained for CD24 and CD103. Scale bars, 20 μm. Arrows indicate cells coexpressing CD24 and CD103 (cDC1). (**J**) Surface area of CD11c$^+$ DC clusters (left) and percentage of scanned area occupied by CD11c$^+$ DC clusters (right). Data are representative of at least two independent experiments. Each dot represents an individual mouse, except for (G), in which each dot represents a well of cells. For (B), n = 10 mice per sex; for (C) to (F), n = 5 mice per sex; and for (H) to (J), n = 3 to 4 mice per sex. Numbers in representative flow plots indicate mean ± SD. *P < 0.05; **P < 0.01; ***P < 0.001; ****P < 0.0001; ns, not significant. For (B), two-tailed unpaired Student's t test was used and for (E) to (F) and (I), one-way ANOVA was used.

DC–T cell interaction (*Nrp2*), and antigen presentation (*Adam23*) (fig. S3B). Conversely, DCs from males expressed a higher level of negative regulators of DC function, such as *Zfp36* (*30*), *Fos* (*31*), and *Cdkn1a* (*32*) in LCs (Fig. 3D) and *Cd74*, *Zfp36*, and *Nfkbia* in CD11b^{hi} cDC2s (fig. S3B).

To validate potential functional differences in skin DCs between males and females, we used an approach to monitor DC migration from tissue to lymphoid organs (*33*). Specifically, we topically applied fluorescein isothiocyanate (FITC) to the skin and measured the accumulation of FITC$^+$ DCs in draining lymph nodes at day 2 after application (*34*). Using this approach, we found that DCs from females had a greater ability to migrate to draining lymph nodes than those from males (Fig. 3E and fig. S3C). Further, within the lymph nodes, FITC$^+$ DCs from females expressed higher levels of the costimulatory molecules CD40 and CD86 and the maturation marker CD83 than did those from males (Fig. 3F and fig. S3C). Next, to determine the major histocompatibility complex class I (MHC-I) antigen presentation capacity of skin-derived cDC1s, we used the ovalbumin (OVA)–specific CD8$^+$ TCR-transgenic T cell (OT-I) system (*35*, *36*). As assessed through expression of the early T cell activation marker CD69, sorted cDC1s from males showed reduced capacity to present OVA (257-264) control peptide at lower unsaturated concentration and prime naïve T cells compared with female-derived cDC1s (Fig. 3G). These results show that within the skin, females have a more dense and activated DC network than do males.

In support of a role for sex hormones in regulating the sex differences of skin T cells, we found that differences in the number of DCs between males and females were not detectable before sexual maturation (fig. S3D). Further, castration of males before sexual maturation restored the number of cDC1s, LCs, and CD11b^{low} cDC2s to female levels, whereas ovariectomy of females had no effect on DC numbers (Fig. 3H and fig. S3E). These results suggested a role for testosterone in the negative regulation of skin DC homeostasis and function. To test this possibility, female mice were treated for 3 weeks with testosterone, which reduced the numbers of cDC1s and CD11b^{low} cDC2s to levels comparable to those observed in males (fig. S3F). Conversely, the number of LCs was only moderately reduced after testosterone treatment, a phenomenon that could be explained by the longevity of LCs within tissue (*37*, *38*).

To visualize sex differences in skin DC density, we performed confocal microscopy of whole-mount ear pinnae of adult females and males (3 to 6 months old). Within the epidermis, and in agreement with a previous report (*39*), the density of LCs was higher in females than in males (Fig. 3, I and J). Within the dermis, skin-resident DCs (visualized by CD11c) were dominantly organized in clusters that were larger in females compared with males (Fig. 3, I and J). In agreement with bias in cell recovery from tissues, differences in DC density between males and females were even more substantial through imaging than after cell extraction. Further characterization of DC subsets revealed that CD11c$^+$ cells coexpressing CD103 and CD24 (cDC1s) were highly enriched in the female DC clusters compared with their male counterparts (Fig. 3I). Thus, the skin of females was characterized by an increase in the density of tissue resident DCs compared with males. Removing male sex hormones by castration increased the density of LCs and the size of DC clusters (Fig. 3, I and J). Our results thus far suggested that within the skin, DCs and T cells may be convergently controlled by sex hormones, and that male sex hormones negatively affect both cell subsets.

DC network homeostasis is associated with ILCs and AR signaling

We next investigated whether the negative effect of androgen signaling on DC homeostasis is direct or indirect. Because skin-resident DCs generally do not express the AR gene (*Ar*) (*40*–*42*) (fig. S4A), we investigated whether the lymphoid compartment could represent a functional target of AR signaling. To this end, we crossed $Ar^{fl/fl}$ mice with $Il7r^{cre}$ mice, a strategy that abolishes the ability of lymphoid cells to respond to androgen signaling. As shown in fig. S4B, sex differences in DC numbers were abolished in $Il7r^{cre}Ar^{fl/fl}$ female and $Il7r^{cre}Ar^{fl/Y}$ male mice, supporting the idea that androgen-imposed sex differences are dependent on AR signaling in lymphocytes.

To identify the potential target(s) of AR signaling, we performed scRNA-seq on skin lymphoid cells in males and females. ILC2s, a dominant population of skin lymphoid cells, expressed the highest level of *Ar* compared with the other lymphoid subsets analyzed (Fig. 4, A and B, and fig. S4, C and D). (*43*, *44*). As described previously, ILC2s dominantly reside within the dermis, and reanalysis of the previous dataset (*45*) revealed that the level of AR was higher in ILC2s from the dermal compartment for both males and females (fig. S4E). Differences in ILC2 numbers and frequencies between males and females were detected in all compartments analyzed: the epidermis, dermis, and subcutaneous adipose tissue (fig. S4F). The expression level of AR was comparable between male and females (Fig. 4B), implying that ILC2s from both males and females are intrinsically programmed to respond to androgens in both sexes. This observation concurs with previous work showing that lung ILC2s express high levels of AR and are negatively affected by androgen signaling (*44*, *45*). Indeed, within the skin, ILC2s also had the highest number of differentially expressed genes between males and females (adjusted P value < 0.05) compared with other lymphoid populations (Fig. 4C). Further, GO enrichment analysis highlighted an increase in pathways associated with T cell and leukocyte activation in female ILC2s compared with those from males (Fig. 4, C and D, and fig. S4G). ILC2s from female skin also expressed a higher level of activation-associated genes such as *Icos*, *Tnfrsf4*, and *Cd81* compared with males, whereas male ILC2s expressed a higher level of immunosuppression-associated genes such as *Fgl2* and *Pik3ip1*, as well as multiple nuclear factor κB inhibitors, including *Nfkbia*, *Nfkbid*, and *Nfkbiz* (Fig. 4D). ILC2s were enriched in the female skin compared with that of males, but only after puberty, and castration of the males restored the number of ILC2s, as well as *Icos* expression and IL-13 production, to levels comparable to those of females (Fig. 4, E and F, and fig. S4H). To assess the potential contribution of cell-intrinsic AR signaling on ILC2s, we analyzed the number of ILC2s in male and female mice with intact or impaired AR signaling only in the lymphoid compartment ($Il7r^{cre}Ar^{fl/fl}$ female and $Il7r^{cre}Ar^{fl/Y}$ male mice). AR depletion in lymphocytes increased the number of ILC2s in males and abolished the differences in ILC2s between males and females (Fig. 4G). These observations pointed to ILC2s as a potential direct target of androgens in the skin and as

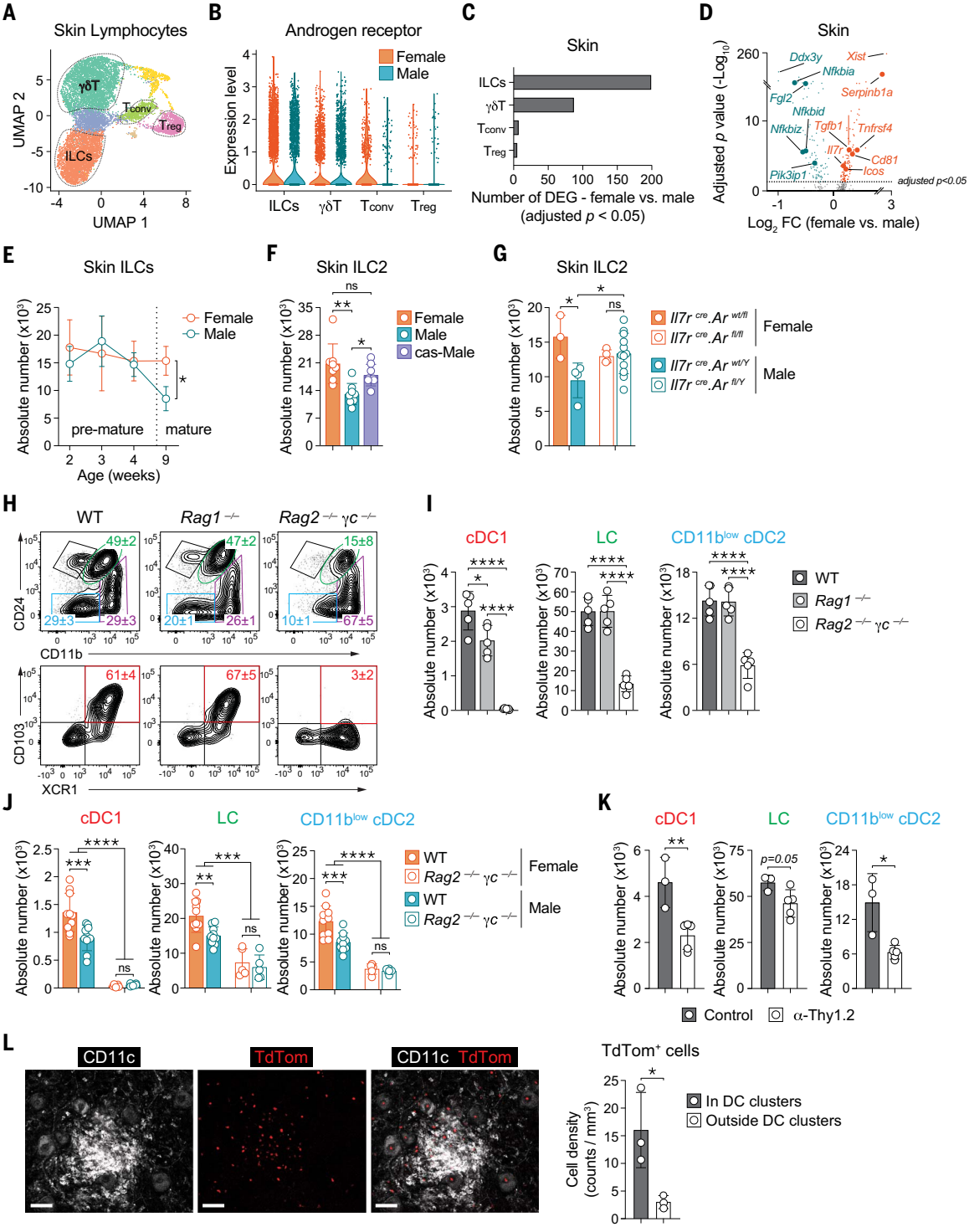

Fig. 4. AR signaling in ILC2s regulates the homeostasis of the skin DC network. (**A** to **D**) Live CD45$^+$ CD90.2$^+$ γδTCR^{hi-} cells from the skin of adult female and male mice were analyzed by scRNA-seq. (A) UMAP projection plot showing the major skin lymphoid cell subsets (cell number: 11,797). (B) Expression levels of the AR gene (*Ar*) in the major skin lymphoid cell subsets. (C) Number of differentially expressed genes in skin lymphoid cell populations between female and male mice, with an adjusted *P* value cutoff of 0.05. (D) Differentially expressed genes in skin ILCs between female and male mice. Highly expressed genes in females are shown in orange, and highly expressed genes in males are shown in teal. (**E**) Absolute numbers of skin ILCs at various ages in female and male mice. (**F** and **G**) Flow cytometry analysis of ILC2s (live CD45$^+$ CD90.2$^+$ γδTCR$^-$ TCRβ$^-$NK1.1$^-$ GATA3$^+$). (F) Absolute numbers of skin ILC2s in adult females, males (sham surgery), and castrated males (cas-Male). (G) Absolute numbers of skin ILC2s in *Il7r*^{cre}*Ar*$^{wt/Y}$, *Il7r*^{cre}*Ar*$^{fl/Y}$, *Il7r*^{cre}*Ar*$^{fl/wt}$ and *Il7r*^{cre}*Ar*$^{fl/fl}$ adult mice. (**H**) Representative contour plots showing frequencies of live CD45$^+$ Lineage$^-$ Ly6C$^-$ CD64$^-$ CD11c$^+$ MHC-II$^+$ DC subsets within the skin of WT, *Rag1*$^{-/-}$, and *Rag2*$^{-/-}$*γc*$^{-/-}$ mice. (**I**) Absolute numbers of cDC1s, LCs, and CD11b^{low} cDC2s within the skin of WT, *Rag1*$^{-/-}$, and *Rag2*$^{-/-}$*γc*$^{-/-}$ mice. (**J**) Absolute numbers of cDC1s, LCs, and CD11b^{low} cDC2s within the skin of WT and *Rag2*$^{-/-}$*γc*$^{-/-}$ female and male mice. (**K**) Absolute numbers of cDC1s, LCs,

and CD11b^{low} cDC2s in the skin of anti-Thy1.2–treated mice and untreated control mice. (**L**) Left: Representative confocal images of whole-mount ear pinnae from Red5 female mice stained for CD11c. TdTom represents cells expressing IL-5. Scale bars, 50 μm. Right: bar graph showing the density of tdTomato^{+} cells within and outside the DC cluster areas. Data are representative of at least two independent experiments. For bar graphs, each dot represents an individual mouse. For (A) to (D) and (I), n = 5 mice per sex; for (E) and (F), n = 8 mice per sex; for (G), n = 3 to 10 mice per sex; for (J), n = 5 to 10 mice for sex; for K, n = 3 to 5 mice per sex; and for (L), n = 3 mice per sex. Numbers in representative flow plots indicate mean ± SD. *P < 0.05; **P < 0.01; ***P < 0.001; ****P < 0.0001; ns, not significant. For (E) and (K) to (L), two-tailed unpaired Student's t test was used; for (F) and (I), one-way ANOVA was used; and for (G) and (J), two-way ANOVA was used.

a likely determinant of skin DC homeostasis and function.

To explore the connection between ILC and DC homeostasis, we compared the DC network of mice with an intact immune system (wild type, WT) with those from mice without an adaptive immune system (*Rag1*$^{-/-}$) or those devoid of both innate and adaptive lymphoid cells (*Rag2*$^{-/-}\gamma c^{-/-}$). Although no differences were observed in DC composition or number between WT and *Rag1*$^{-/-}$ mice, the DC skin network was profoundly disrupted in *Rag2*$^{-/-}\gamma c^{-/-}$ mice compared with WT and *Rag1*$^{-/-}$ mice, with a substantial reduction in cell numbers of cDC1s (WT versus *Rag2*$^{-/-}\gamma c^{-/-}$: fold change >15), LCs (WT versus *Rag2*$^{-/-}\gamma c^{-/-}$: fold change >2.5), and CD11b^{low} cDC2 (WT versus *Rag2*$^{-/-}\gamma c^{-/-}$: fold change >2.5) (Fig. 4, H and I, and fig. S4, I and J). Further, the remaining DCs in *Rag2*$^{-/-}\gamma c^{-/-}$ mice were present in similar numbers between males and females (Fig. 4J and fig. S4K). These results support the idea that in the absence of ILCs, DC homeostasis is profoundly affected and DC sex bias is no longer observed. Because defects in cytokine signaling mediated by receptors containing the γc chain could affect numerous biological processes in *Rag2*$^{-/-}\gamma c^{-/-}$ mice, we addressed the direct contribution of ILCs to the phenomenon observed. Depletion of ILCs in *Rag1*$^{-/-}$ females using anti-Thy1.2 decreased the number of cDC1s and CD11b^{low} cDC2s and had a slight effect on LCs (Fig. 4K and fig. S4L). Consistent with a divergent control of CD11b^{hi} cDC2s, this subset was not affected (fig. S4L). A functional link between ILC2 and DC homeostasis was further supported by the observation that ILC2s [visualized with Red5/IL-5^{tdTomato} (*46*)] were enriched within DC clusters (Fig. 4L). These data support a functional link among ILC2s, androgen signaling, and the three major DC skin subsets.

ILC2s control cDC1 homeostasis in a granulocyte-macrophage colony-stimulating factor–dependent manner

We performed adoptive transfer experiments to determine whether ILC2s could be sufficient to control the skin DC network. Skin ILC2s were sorted and expanded in vitro in the presence of IL-7, IL-2, thymic stromal lymphopoietin (TSLP), and IL-18 (*47*) before intradermal injection in female *Rag2*$^{-/-}\gamma c^{-/-}$ mice. At 7 days after injection, local delivery of ILC2s increased cDC1s within the skin of *Rag2*$^{-/-}\gamma c^{-/-}$ mice compared with control *Rag2*$^{-/-}\gamma c^{-/-}$ mice exhibiting a disrupted DC network (Fig. 5A). ILC2 injection within the dermis of *Rag2*$^{-/-}\gamma c^{-/-}$ mice also moderately increased the number of LCs in the skin (fig. S5A). Thus, direct deposit of ILC2s in the skin of mice with a disrupted DC network is sufficient to restore the cDC1 compartment and partially restore LCs.

Our model thus far suggested that ILC2 number and function are negatively affected by local androgen signaling. Because ILC2s from males and females expressed a comparable level of AR (Fig. 4B), purified and expanded ILC2s from males and females (equally mixed) were injected intradermally in both male and female *Rag2*$^{-/-}\gamma c^{-/-}$ mice. In support of a negative role for local androgens, the frequencies of cDC1s induced by ILC2 deposition were lower in males than in females (Fig. 5B).

We then explored the mechanisms by which ILC2s may be able to control DC homeostasis, focusing on the potential link between ILC2-derived granulocyte-macrophage colony-stimulating factor (GM-CSF) and cDC1s. Previous work uncovered a nonredundant role for GM-CSF in cDC1 homeostasis and survival (*48*, *49*), and in agreement with this, GM-CSF receptors (*Csf2ra* and *Csf2rb*) were expressed in all skin DCs, including cDC1s (fig. S5B). Further, cDC1s were substantially decreased within the skin of both GM-CSF– and GM-CSF receptor–deficient mice (Fig. 5C). Abrogation of GM-CSF production by hematopoietic cells using *Vavi*^{icre} also confirmed the nonredundant role of GM-CSF on cDC1 homeostasis within the skin (fig. S5, C and D).

Although GM-CSF can be produced by various cell subsets, ILCs can represent a major source of this cytokine. For instance, within the gut, ILC3-derived GM-CSF can control DC number and function (*50*–*52*). Both human and murine ILC2s have been shown to produce GM-CSF (*53*–*55*). Using GM-CSF reporter mice (*Csf2*$^{flox–tdTomato}$), we found that within the skin, most ILC2s expressed GM-CSF in both males and females, albeit at a slightly higher frequency in females (Fig. 5D). Coupled with the higher number of ILC2s in females, this translated to a higher absolute number of GM-CSF–producing ILC2s in the skin of females compared with males (Fig. 5D). Whereas this observation did not imply reduced overall GM-CSF in males compared with females, it did suggest differences in a dominant subset of GM-CSF–producing cells that were in close proximity to skin DCs within the dermis.

We next tested the possibility that ILC2-derived GM-CSF could be sufficient to control skin cDC1s. Skin ILC2s from WT or *Csf2*$^{-/-}$ mice were sorted and expanded in vitro before intradermal delivery to *Rag2*$^{-/-}\gamma c^{-/-}$ mice. At 7 days after skin delivery, WT ILC2s increased the frequency and absolute number of cDC1s within the skin compared with controls (Fig. 5E). Conversely, ILC2s purified from *Csf2*$^{-/-}$ mice failed to restore cDC1s within the skin. Thus, ILC2-derived GM-CSF is sufficient to promote the local accumulation of cDC1s in the skin.

Our results suggest that negative regulation of ILC2s by androgens leads to reductions in DC accumulation and activation within the skin, which subsequently results in reduced local immunity in the skin of males compared with females (Fig. 5F). Further, our findings show that tissue immune set point and DC network strength are fundamentally defined by the dual action of sex hormones and the microbiota, with sex hormones controlling the strength of local immunity and microbiota calibrating its tone.

Discussion

The profound reliance of the skin DC network on ILC2s, which are themselves under the tight control of sex hormones, provides a fundamental framework with which to understand the differences in tissue immunity between males and females. Our work here also suggests that sexual dimorphism within the skin is dominantly controlled by the strength of the resident DC network, with marked differences in the density and activation of defined subsets of DCs within the skin of females compared with males.

Our data indicate that a single cell subset, ILC2s, contributes to sex immune bias within the skin. In our settings, ILC2s and ILC2-derived GM-CSF primarily restored cDC1s. However, other DC subsets, such as LCs and CD11b^{low} cDC2s, were also affected by sex, and removal of ILCs from RAG mice had an effect on both of these DC subsets. The fact that ILC2 transfer dominantly restored cDC1s and no other DC subsets may indicate that further activation of ILC2s in the tissue may be required for the development and survival of other DC subsets. Indeed, type 2 cytokines, which can be abundantly produced by ILC2s, have been shown to contribute to LC and CD11b^{low} cDC2 homeostasis (*24*, *56*, *57*). Thus, the ability of ILC2s to produce numerous factors associated with DC homeostasis could explain the broad

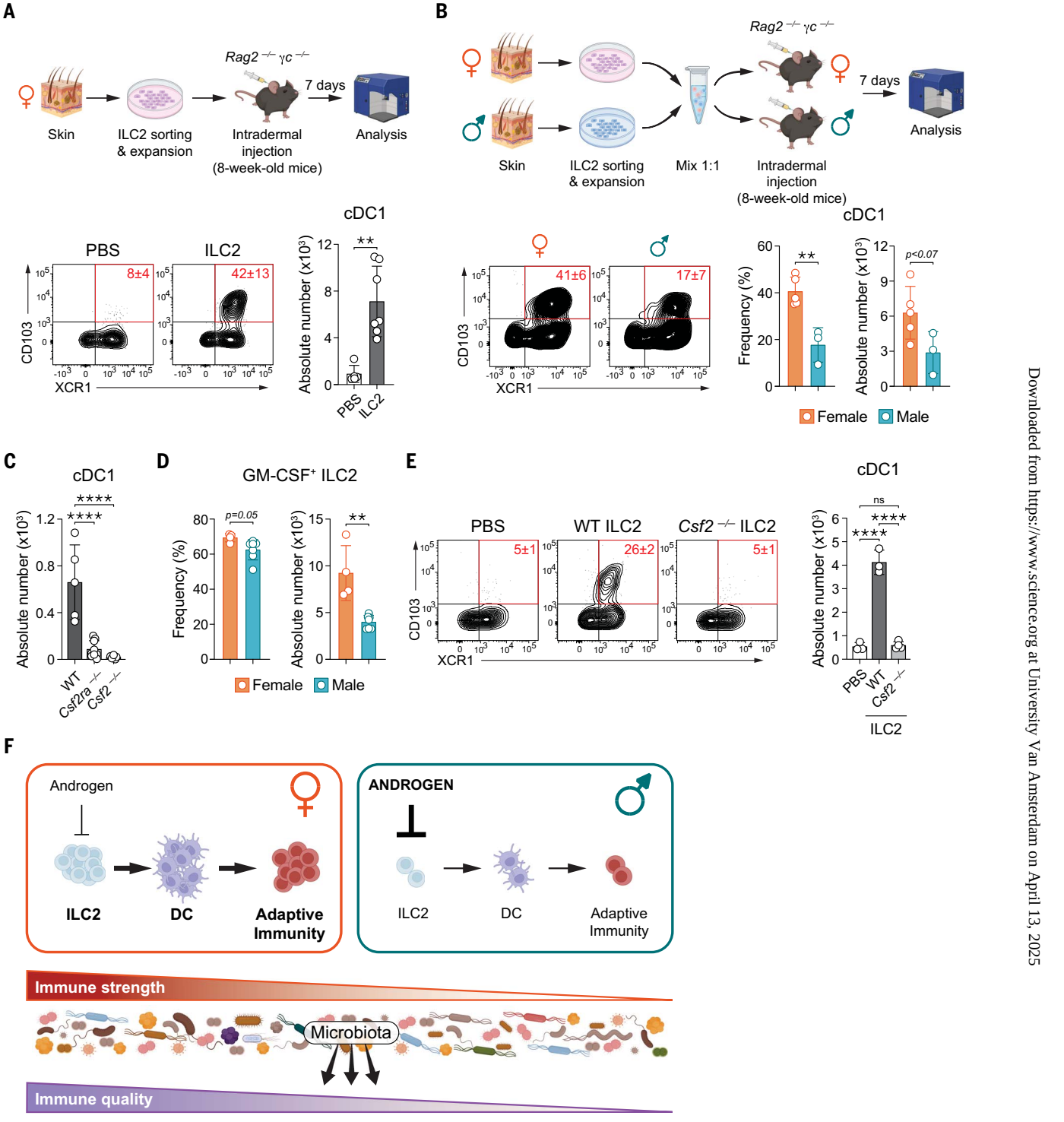

Fig. 5. ILC2s control cDC1 in a GM-CSF–dependent manner. (**A**) Skin ILC2s were sorted, expanded in vitro, and intradermally injected in adult *Rag2*$^{-/-}\gamma c^{-/-}$ female mice. Control mice received PBS. Skin DC subsets were analyzed at day 7 after injection. Representative contour plots show cDC1s within the skin of PBS- and ILC2-injected *Rag2*$^{-/-}\gamma c^{-/-}$ females. Bar graphs show absolute numbers of cDC1s. (**B**) Cultured ILC2s sorted from the skin of adult female and male mice were equally mixed and intradermally injected into adult *Rag2*$^{-/-}\gamma c^{-/-}$ female and male mice. Skin cDC1s were then analyzed by flow cytometry. Representative contour plots show cDC1s within the skin of *Rag2*$^{-/-}\gamma c^{-/-}$ female and male mice after injection of ILC2s. Bar graph shows the frequencies and absolute numbers of live CD45^{+} Lineage^{-} Ly6C^{-} CD64^{-} CD11c^{+} MHC-II^{+} CD24^{+} CD11b^{low} CD103^{+} cDC1s in the skin. (**C**) Absolute numbers of skin ILC2s in WT, *Csf2ra*$^{-/-}$, and *Csf2*$^{-/-}$ mice. (**D**) Frequencies and absolute numbers of skin GM-CSF^{+} ILC2s (gating at live CD45^{+} CD90.2^{+} γδTCR^{-} TCRβ^{-} NK1.1^{-} GATA3^{+} tdTomato^{+}) in adult *Csf2*$^{flox-tdTomato}$ female and male mice. (**E**) Left: representative contour plots of skin cDC1s in adult *Rag2*$^{-/-}\gamma c^{-/-}$ females injected with PBS, ILC2s from WT females, or ILC2s from *Csf2*$^{-/-}$ females. Right: absolute numbers of skin cDC1s in *Rag2*$^{-/-}\gamma c^{-/-}$ females injected with PBS, ILC2s from WT females, or ILC2s from *Csf2*$^{-/-}$ females. (**F**) Model of the role of androgen-DC-ILC2 axis in shaping sex dimorphism of skin immunity. Data are representative of at least two

independent experiments. Each dot represents an individual mouse. For (A), n = 5 to 7 mice per sex; for (B), n = 3 to 5 mice per sex; for (C), n = 5 to 10 mice per sex; for (D), n = 4 to 8 mice per sex; and for (E), n = 3 to 4 mice per sex. Numbers in flow plots indicate mean ± SD. *P < 0.05; **P < 0.01; ***P < 0.001; ****P < 0.0001; ns, not significant. For (A), (B), and (D), two-tailed unpaired Student's t test was used; for (C) and (E), one-way ANOVA was used.

impact of these cells on the strength of the DC network.

The strong impact of androgens on ILC2 homeostasis, a phenomenon previously reported within the lung (*43*, *58*), allows male sex hormones to broadly affect the local immune system through the regulation of a single cell subset. ILCs have been shown to play an important role in the regulation of tissue physiology through their ability to bridge numerous biological systems (*59*). Here, we found that the intrinsic ability of ILC2s to link the immune system with the endocrine system plays a fundamental role in shaping immune sexual dimorphism.

Our data also support the idea that the degree to which each tissue may be shaped by sex is highly tissue dependent. Among the three major barrier sites explored, we found that skin immunity was the most affected by sex differences. These findings are consistent with a previous study revealing that among 44 human tissues analyzed, the skin expressed the highest number of sex-biased genes (*60*). Our findings in the skin are in contrast to those in the gut, where immune differences between males and females were not observed, and to the lung, where the microbiota was required to impose sex-biased tissue immunity. These observations have important implications for our understanding of differences in disease etiology and tropism between males and females.

Although sex bias in tissue physiology can result from complex interactions between sex chromosome gene products and sex hormones, we found that within the skin, sex hormones, in particular androgens, play a dominant role in shaping immune homeostasis and responses to the microbiota. This dominant role for sex hormones in shaping skin immunity could be explained by the fact that the skin is itself an important endocrine organ (*61*, *62*). Keratinocytes may synthesize androgens de novo from cholesterol or by converting circulating weaker androgens to more potent ones. For example, the 5α-reductases are highly expressed in keratinocytes and sebocytes, which can convert testosterone to 5α-dihydrotestosterone, a much more potent and stable agonist of the AR (*63*). This fundamental property of the skin associated with potent local androgen signaling may, at least in part, explain the dominant role of androgens in defining immune threshold within the skin.

Whereas immune sexual dimorphism has been mostly highlighted in the context of inflammatory disorders and autoimmunity, bias in host immunity may serve the purpose of protecting fundamental sex-specific processes such as pregnancy or lactation. Therefore, it is worth noting that constitutive enrichment of ILC2s in females also contributes to female reproductive function. Indeed, ILC2s are highly increased during pregnancy in the uterus, both in humans and in mice, and play a role in controlling the timing of labor onset (*64*, *65*). Whether heightened ILC2s and associated enhanced immunity in females also serve the fundamental purpose of protecting fetal life remains to be investigated.

Our data reveal that in contrast to the lung, the microbiota was not necessary for imposing sex-biased immune differences within the skin. We found that the presence of the microbiota further shaped sex-biased immune differences by enhancing type 17 programs, a class of immune response that we and others have previously shown to promote tissue antimicrobial function and regeneration (*19*, *66*, *67*). Therefore, remodeling of hormonally controlled tissue immunity by the microbiota toward a type 17 program in females may allow microbial partners to enhance their positive effect on host physiology in a sex-specific manner. The ability of the microbiota to shape sex bias toward type 17 and/or T_{reg} immunity in the skin is independent of microbiota exposure early in life. The ability of the microbiota to affect the sex-biased immune landscape highlights the integrated impact of both internal (hormonal) and external (microbiota) factors in ultimately shaping tissue immunity. Previous work revealed that the gut microbiota from males is able to enhance testosterone levels, and the skin microbiota undergoes a profound remodeling at puberty (*16*, *68*). Whether a hormone-induced shift in the microbiota and microbiota control of hormonal levels also contributes to differences in disease intensity and tropism remains to be addressed. Because of the complex etiology of inflammatory disorders, how hormonal control of tissue immunity is sustained under chronic settings needs further exploration. More generally, how our findings apply to humans needs to be addressed. Based on the known sexual dimorphism in skin and skin-related diseases in humans (*3*, *69*–*79*), we believe that our finding of heightened DC function and numbers in females may provide one possible explanation for such differences.

Our work further supports the concept that understanding health and disease requires the integration of the fundamental impact of sex on immune function and how each tissue may be differentially controlled and affected. Our findings that androgen-mediated control of a single cell subset can be sufficient to control the density and activation of the DC network within the skin opens the door for developing therapeutic approaches targeting local control of sex hormones as potential adjuvants or regulators of local immunity.

Materials and methods

Mice

Specific pathogen–free C57BL/6NTac, Red5, *Rag1*$^{-/-}$, *Rag2*$^{-/-}\gamma c^{-/-}$ mice were obtained from The Jackson Laboratory and Taconic Biosciences. Germ-free C57BL/6NTac mice were bred and maintained in the National Institute of Allergy and Infectious Diseases (NIAID) Microbiome Program gnotobiotic animal facility. *Rag1*$^{-/-}$ mice are deficient in recombination-activating genes 1 (RAG1), which is essential regulator of genes that encode immunoglobulin and the T cell receptor (TCR). *Rag1*$^{-/-}$ mice do not have mature B and T lymphocytes but do have ILCs (*80*). *Rag2*$^{-/-}\gamma c^{-/-}$ mice are deficient in recombination-activating genes 2 (RAG2) and the IL-2 receptor subunit gamma, which caused a deficiency of ILCs, T cells, and B cells (*81*). *Csf2*$^{\text{flox-tdTomato}}$ and *Vav1*$^{\text{iCre}}$ *Csf2*$^{\text{flox-tdTomato}}$ mice were recently described (*82*). *Csf2ra*$^{-/-}$ mice were generated by Dr. Manfred Kopf at ETH Zürich (*83*). OT-I OVA-specific CD8^{+} TCR transgenic mice were provided by Dr. Andrea Pichler from Dr. Pamela Schwartzberg's laboratory, who obtained them from Taconic Biosciences. *Csf2*$^{-/-}$ mice were provided by Dr. Camille Spinner in Dr. Vanja Lazarevic's laboratory. *Il7r*$^{\text{cre}}$*Ar*$^{\text{fl/fl}}$ (female) and *Il7r*$^{\text{cre}}$*Ar*$^{\text{fl/Y}}$ (male) mice were provided by Jean-Charles Guéry. Wildling mice were offspring of a colony of C57BL/6 mice reconstituted with wild mouse–derived microbiota and pathogens (*17*), and were provided by Dr. Barbara Rehermann. All mice were bred and maintained at an American Association for the Accreditation of Laboratory Animal Care (AAALAC)–accredited animal facility at NIAID, the National Cancer Institute, or the National Institute of Diabetes and Digestive and Kidney Diseases (NIDDK) and housed in accordance with procedures outlined in the National Institutes of Health's *Guide for the Care and Use of Laboratory Animals*. All mice were provided a standard pelleted rodent diet and tap water ad libitum under the following environmental conditions: ambient temperature (20 to 24°C), 40 o 70% humidity, and 12 hour/12 hour (7:00 am/7:00 pm) light/dark cycle. Mice were euthanized by CO_2 exposure

using an euthanasia chamber linked to a compressed CO_2 gas tank allowing gas flow into the chamber to be regulated (100% CO_2 at a rate in liters/minute to displace 30% of the euthanasia chamber volume). The euthanasia procedure complies with the institutional Animal Research Advisory Committee (ARAC) and the American Veterinary Medical Association (AVMA) guidelines on euthanasia of rodents. All experiments were performed at NIAID under an animal study proposal (LHIM-3E) approved by the NIAID Animal Care and Use Committee. In-house breeder offspring were weaned at 3 weeks after birth. Age-matched adult female and male mice (~2 to 3 months old) were used in each experiment unless specified otherwise.

Bacteria and fungi culture and topical association

S. epidermidis NIHLM087 was cultured for 6 to 7 hours in tryptic soy broth at 37°C without shaking to reach an optical density at 600 nm (OD_{600}) of 0.8. *C. accolens* strain ATCC 49725 was cultured for 18 hours in a brain-heart infusion broth supplemented with 1% Tween 80 (Sigma-Aldrich) at 37°C with shaking. *C. albicans* (a strain isolated from an IL-22-knockout mouse) (*84*) was grown in tryptic soy broth at 30°C with shaking for 18 hours. The bacterial or fungal suspension was topically applied to the mice across the surface of the ear pinnae and the rest of the body using a sterile cotton swab. Topical association of bacteria or fungi was performed every other day for a total of four times for each experiment. Immune responses were analyzed at day 14 after the first association. In this model, the bacteria and fungi colonize at the surface but do not infect mice or cause inflammation, as we described previously (*18*–*21*).

S. aureus infection

S. aureus 42F02 was cultured in tryptic soy broth at 37°C with shaking for 3 to 4 hours to reach an OD_{600} of 0.8 [~2×10^8 colony-forming units (CFU)/ml]. *S. aureus* was washed with phosphate-buffered saline (PBS), diluted to 1×10^7 CFU/ml, and then 15 μl of the suspension was intradermally injected into each side of ears of 8- to 9-week-old female and male mice. Immune responses were analyzed at day 7 after infection.

Tissue processing

Murine tissues were processed to isolate cells as described previously (*18*, *85*). Briefly, mice were euthanized with CO_2, and ear pinnae, small intestine lamina propria (siLP), lung, and draining lymph nodes were collected after perfusing with 20 ml of cold PBS. Ears were separated into ventral and dorsal sheets and then digested in the media with DNase and Liberase TL (RPMI 1640 media with 2 mM L-glutamine, 1 mM sodium pyruvate, and nonessential amino acids, 55 mM β-mercaptoethanol, 20 mM HEPES, 100 U/ml penicillin, 100 mg/ml streptomycin, 0.5 mg/ml Dnase, and 0.25 mg/ml Liberase TL purified enzyme blend) at 37°C for 1 hour and 45 min. Digested ears were homogenized and filtered through a 50-μm cell strainer. For the lung, tissues were excised and digested in the media with DNase (0.5 mg/ml) and Liberase TL (0.1 mg/ml) at 37°C for 30 min. Digested lungs were smashed and filtered through 70-mm cell strainer. For the siLP, the Peyer's patches were first removed and then small intestines were opened and washed with cold PBS to remove luminal contents. Tissues were incubated with media containing 5 mM EDTA and 0.145 mg/ml dithiothreitol for 20 min at 37°C and then digested with DNase (0.5 mg/ml) and Liberase TL (0.1 mg/ml) at 37°C for 25 min. Leukocytes in lung and siLP were enriched using 37.5% Percoll. Cell suspensions were washed with PBS and were then ready for downstream analysis.

In vitro restimulation

To assess cytokine production potential of skin immune cells, single-cell suspensions were cultured in complete medium (RPMI 1640 supplemented with 2 mM L-glutamine, 1 mM sodium pyruvate and nonessential amino acids, 20 mM HEPES, 100 U/ml penicillin, 100 μg/ml streptomycin, 50 mM β-mercaptoethanol, and 10% fetal bovine serum) containing restimulation reagent mixture [50 ng/ml phorbol myristate acetate (Sigma-Aldrich), 5 mg/ml ionomycin (Sigma-Aldrich), and a 1:1000 dilution of GolgiPlug (BD Biosciences)] for 2.5 hours at 37°C in 5% CO_2.

Flow cytometry analysis

Single-cell suspensions were incubated with 4′,6-diamidino-2-phenylindol (DAPI, Sigma-Aldrich) or LIVE/DEAD Fixable Blue Dead Cell for 15 min on ice to exclude dead cells. To stain surface markers, single-cell suspensions were incubated with fluorophore-conjugated antibodies (listed in table S1) in the presence of purified anti-mouse CD16/32 and purified rat gamma globulin for 30 min at 4°C. After surface staining and washing, cells were fixed and permeabilized using the Foxp3/Transcription Factor Staining Buffer Set (ThermoFisher Scientific) for 1 hour at 4°C, and fixed cells were incubated with fluorophore-conjugated antibodies for at least 1 hour at 4°C to stain intracellular cytokines and transcription factors. Data were acquired using a BD Fortessa X-20 flow cytometer with FACSDiVa software (BD Biosciences), and data analysis was performed with FlowJo software (TreeStar).

In vivo treatment with blocking antibodies

Female *Rag1*$^{-/-}$ mice were intraperitoneally injected with 2 mg of anti-mouse Thy1.2 antibody (clone 30H12; BioXCell) every 2 days for a total of four times. Effects on skin immune cells were analyzed at day 12 after the first injection.

Castration and ovariectomy

Ovariectomized females and some castrated males were ordered from The Jackson Laboratory. Castration was also performed on site following the instructions in a published protocol (*86*). Sham surgery was performed on control mice. Surgeries were performed at 3 to 4 weeks of age.

Testosterone treatment

Testosterone propionate was dissolved into corn oil and intraperitoneally injected to ~3- to 4-week-old female mice at 15 mg/kg body weight. Testosterone injection was performed every 3 days for up to 3 weeks. Mice in control groups were injected with an equal volume of corn oil.

FITC topical treatment

FITC isomer 1 (ThermoFisher, L09319.MF) was dissolved in equal volumes of acetone and dibutyl phthalate (Sigma-Aldrich) to the concentration of 0.6 mg/ml and applied to the ear skin of 8-week-old females and males in 15-μl aliquots with a pipette tip. The number of $FITC^+$ DCs was evaluated by flow cytometry at day 2 after treatment.

OT-I antigen presentation assay

OT-I naïve $CD8^+$ T cells were purified from spleen using a naïve $CD8^+$ T cell isolation kit (Miltenyi, 130-096-543) and labeled with carboxyfluorescein diacetate succinimidyl ester. Single-cell suspensions of ear skin of WT female and male C57BL/6 mice (8 to 9 weeks old) were stained with antibodies against CD24, CD103, CD45, CD64, CD11c, CD11b, MHC-II, Ly6C, lineage (TCRβ, γδTCR, Ly6G, CD45R, NK1.1), and DAPI on ice for 30 min. Skin cDC1s were sorted as the $DAPI^-$ $CD45^+$ $Lineage^-$ $Ly6C^-$ $CD64^-$ $CD11c^+$ MHC-II^+ $CD24^+$ $CD11b^{low}$ $CD103^+$ population on a Sony MA900 cell sorter with a 100-mm chip. Sorted cDC1s were incubated with different concentrations of OVA (254-267) peptide (1 or 10 μg/ml) for 4 hours, washed extensively, and incubated with OT-I $CD8^+$ T cells in a 1:10 ratio. After 18 hours, activation of T cells was analyzed by CD69 expression.

Imaging by confocal microscopy

Mouse ears were cut and separated into ventral and dorsal sheets and then fixed overnight in 1% paraformaldehyde in PBS at 4°C. After washing with PBS, samples were blocked in 1% bovine serum albumin plus 0.25% Triton X-100 blocking buffer for 2 hours at room temperature. Antibodies were added to samples in a blocking buffer to stain for 24 to 36 hours. Then, samples were washed with PBS and mounted in ProlongGold. After drying for

16 hours, images were captured with a Leica TCS SP8 confocal microscope equipped with HyD and PMT detectors and a 20× oil objective (HC PL APO 40×/1.3 oil). Images were analyzed using Imaris software (Bitplane). The DC clusters were quantified using surface analysis tool in Imaris and the volum was selected based on the intensity of the magenta channel. Clusters were defined as those >2.84e4 voxels. For LC quantification, 20 × 20 μm areas were selected from different positions of each scanned sample and the number of LCs was determined.

ILC2 sorting, in vitro expansion, and intradermal injection

Single-cell suspensions of ear skin of WT C57BL/6 or *Rag1*$^{-/-}$ mice were stained with antibodies against CD127, CD218α, CD45, Thy1.2, lineage (TCRβ, γδTCR, Ly6G, Ly6C, CD11b, CD11c, CD45R, CD3, CD19, NK1.1, FcεR1α, CD49f), and DAPI on ice for 30 min. Skin ILC2s were sorted as the DAPI$^-$ CD45$^+$ Thy1.2$^+$ Lineage$^-$ CD127$^+$ CD218α$^+$ population on a Sony MA900 cell sorter with a 100-mm chip. Sorted ILC2s were cultured and expanded in complete medium with IL-7 (25 ng/mL), IL-2 (25 ng/mL), IL-18 (50 ng/mL), and TSLP (50 ng/mL). ILC2s were intradermally injected to *Rag2*$^{-/-}\gamma c^{-/-}$ mice at the level of 0.2 to 0.5 million cells per ear. Effects of ILC2s were evaluated at day 7 after injection.

Keratinocyte purification and bulk RNA-seq

Epidermal keratinocytes were sorted and sequenced as described previously (*87*). Briefly, cell suspension from ears of mice at day 14 after *S. epidermidis* application were stained using the following antibodies: anti-CD16/32 (93), anti-CD31 (MEC13.3), anti-CD34 (RAM34), anti-CD45 (30-F11), anti-CD49f (eBioGoH3), and anti-Sca-1 (D7) in the presence of DAPI. Keratinocytes were sorted by a Sony MA900 cell sorter with a 100-mm chip as DAPI$^-$ CD45$^-$ CD31$^-$ CD34$^-$ CD49f$^+$ Sca-1$^+$ cells. Then, RNA was extracted using the Qiagen MicroRNA kit (Qiagen) following the manufacturer's instructions, and a sequencing library was prepared using the Ovation SoLo RNA-Seq library preparataion kit (Tecan) following the manufacturer's instructions. Sequencing was performed on a NextSeq 500 using the High Output kit. Sequencing reads were mapped to the C57BL/6 mouse genome (GRCm38: mm10) and differential gene expression was calculated using DESeq2 (*88*). Differentially expressed genes (adjusted $P < 0.05$) were used for GO enrichment analysis (*89*).

scRNA-seq and transcriptome analysis

Skin lymphocytes (CD45$^+$ Thy1.2$^+$, exclude γδTCR^{hi} population) or skin DCs (CD45$^+$ Lin$^-$ Ly6G$^-$ Siglec-F$^-$ CD11c$^+$ MHC-II$^+$) from 8- to 9-week-old female and male mice ($n = 5$ for each sex) were sorted from samples labeled with TotalSeqA hashtags antibodies (BioLegend) on a Sony MA900 cell sorter. All DC and T cell samples were pooled together in two separate vials, and 45,000 cells were loaded to a Chromium Single Cell Controller (10X Genomics) to encapsulate cells into droplets. Libraries were prepared using a Chromium Single Cell 3 Reagent Kits v3 (10X Genomics) following the manufacturer's instructions, and the HTO library was prepared as described previously (*90*). Libraries were then sequenced on an Illumina Nextseq500 (Next Seq 500/550 High Output Kit v2, Illumina). Data were filtered and mapped to the mm10 reference genome by using Cellranger 6.1.1 (10X Genomics). Data were normalized in Seurat and displayed as a uniform manifold approximation and projection (UMAP). Gene expression was compared between females and males using the Seurat FindMarkers function.

Statistical analysis

Groups were compared using Prism software (version 9.5.1). The statistical methods used are described in the figure legends.

REFERENCES AND NOTES

1. S. L. Klein, K. L. Flanagan, Sex differences in immune responses. *Nat. Rev. Immunol.* **16**, 626–638 (2016). doi: 10.1038/nri.2016.90; pmid: 27546235
2. E. P. Scully, J. Haverfield, R. L. Ursin, C. Tannenbaum, S. L. Klein, Considering how biological sex impacts immune responses and COVID-19 outcomes. *Nat. Rev. Immunol.* **20**, 442–447 (2020). doi: 10.1038/s41577-020-0348-8; pmid: 32528136
3. W. Chen, M. Mempel, C. Traidl-Hofmann, S. Al Khusaei, J. Ring, Gender aspects in skin diseases. *J. Eur. Acad. Dermatol. Venereol.* **24**, 1378–1385 (2010). doi: 10.1111/j.1468-3083.2010.03668.x; pmid: 20384686
4. A. L. Fink, K. Engle, R. L. Ursin, W.-Y. Tang, S. L. Klein, Biological sex affects vaccine efficacy and protection against influenza in mice. *Proc. Natl. Acad. Sci. U.S.A.* **115**, 12477–12482 (2018). doi: 10.1073/pnas.1805268115; pmid: 30455317
5. I. Mohammad *et al.*, Estrogen receptor α contributes to T cell-mediated autoimmune inflammation by promoting T cell activation and proliferation. *Sci. Signal.* **11**, eaap9415 (2018). doi: 10.1126/scisignal.aap9415; pmid: 29666308
6. A. Trigunaite, J. Dimo, T. N. Jørgensen, Suppressive effects of androgens on the immune system. *Cell. Immunol.* **294**, 87–94 (2015). doi: 10.1016/j.cellimm.2015.02.004; pmid: 25708485
7. H. Kwon *et al.*, Androgen conspires with the CD8$^+$ T cell exhaustion program and contributes to sex bias in cancer. *Sci. Immunol.* **7**, eabq2630 (2022). doi: 10.1126/sciimmunol.abq2630; pmid: 35420889
8. X. Guan *et al.*, Androgen receptor activity in T cells limits checkpoint blockade efficacy. *Nature* **606**, 791–796 (2022). doi: 10.1038/s41586-022-04522-6; pmid: 35322234
9. C. Yang *et al.*, Androgen receptor-mediated CD8$^+$ T cell stemness programs drive sex differences in antitumor immunity. *Immunity* **55**, 1268–1283.e9 (2022). doi: 10.1016/j.immuni.2022.05.012; pmid: 35700739
10. A. L. Byrd, Y. Belkaid, J. A. Segre, The human skin microbiome. *Nat. Rev. Microbiol.* **16**, 143–155 (2018). doi: 10.1038/nrmicro.2017.157; pmid: 29332945
11. H. Dao Jr., R. A. Kazin, Gender differences in skin: A review of the literature. *Gend. Med.* **4**, 308–328 (2007). doi: 10.1016/S1550-8579(07)80061-1; pmid: 18215723
12. J. W. McCallister, J. G. Mastronarde, Sex differences in asthma. *J. Asthma* **45**, 853–861 (2008). doi: 10.1080/02770900802444187; pmid: 19085573
13. M. Oliva *et al.*, The impact of sex on gene expression across human tissues. *Science* **369**, eaba3066 (2020). doi: 10.1126/science.aba3066; pmid: 32913072
14. J. C. Clemente, L. K. Ursell, L. W. Parfrey, R. Knight, The impact of the gut microbiota on human health: An integrative view. *Cell* **148**, 1258–1270 (2012). doi: 10.1016/j.cell.2012.01.035; pmid: 22424233
15. Y. Belkaid, T. W. Hand, Role of the microbiota in immunity and inflammation. *Cell* **157**, 121–141 (2014). doi: 10.1016/j.cell.2014.03.011; pmid: 24679531
16. J. G. Markle *et al.*, Sex differences in the gut microbiome drive hormone-dependent regulation of autoimmunity. *Science* **339**, 1084–1088 (2013). doi: 10.1126/science.1233521; pmid: 23328391
17. S. P. Rosshart *et al.*, Laboratory mice born to wild mice have natural microbiota and model human immune responses. *Science* **365**, eaaw4361 (2019). doi: 10.1126/science.aaw4361; pmid: 31371577
18. S. Naik *et al.*, Compartmentalized control of skin immunity by resident commensals. *Science* **337**, 1115–1119 (2012). doi: 10.1126/science.1225152; pmid: 22837383
19. S. Naik *et al.*, Commensal-dendritic-cell interaction specifies a unique protective skin immune signature. *Nature* **520**, 104–108 (2015). doi: 10.1038/nature14052; pmid: 25539086
20. J. L. Linehan *et al.*, Non-classical immunity controls microbiota impact on skin immunity and tissue repair. *Cell* **172**, 784–796.e18 (2018). doi: 10.1016/j.cell.2017.12.033; pmid: 29358051
21. V. K. Ridaura *et al.*, Contextual control of skin immunity and inflammation by *Corynebacterium*. *J. Exp. Med.* **215**, 785–799 (2018). doi: 10.1084/jem.20171079; pmid: 29382696
22. S. Tamoutounour *et al.*, Keratinocyte-intrinsic MHCII expression controls microbiota-induced Th1 cell responses. *Proc. Natl. Acad. Sci. U.S.A.* **116**, 23643–23652 (2019). doi: 10.1073/pnas.1912432116; pmid: 31672911
23. M. R. Bell, Comparing postnatal development of gonadal hormones and associated social behaviors in rats, mice, and humans. *Endocrinology* **159**, 2596–2613 (2018). doi: 10.1210/en.2018-00220; pmid: 29767714
24. J. U. Mayer *et al.*, Homeostatic IL-13 in healthy skin directs dendritic cell differentiation to promote T_H2 and inhibit T_H17 cell polarization. *Nat. Immunol.* **22**, 1538–1550 (2021). doi: 10.1038/s41590-021-01067-0; pmid: 34795444
25. A. Weckel *et al.*, Long-term tolerance to skin commensals is established neonatally through a specialized dendritic cell subgroup. *Immunity* **56**, 1239–1254.e7 (2023). doi: 10.1016/j.immuni.2023.03.008; pmid: 37028427
26. V. Pasham *et al.*, OSR1-sensitive regulation of Na+/H+ exchanger activity in dendritic cells. *Am. J. Physiol. Cell Physiol.* **303**, C416–C426 (2012). doi: 10.1152/ajpcell.00420.2011; pmid: 22648948
27. C. J. Henry, D. A. Ornelles, L. M. Mitchell, K. L. Brzoza-Lewis, E. M. Hiltbold, IL-12 produced by dendritic cells augments CD8+ T cell activation through the production of the chemokines CCL1 and CCL17. *J. Immunol.* **181**, 8576–8584 (2008). doi: 10.4049/jimmunol.181.12.8576; pmid: 19050277
28. D. Y. Ma, E. A. Clark, The role of CD40 and CD154/CD40L in dendritic cells. *Semin. Immunol.* **21**, 265–272 (2009). doi: 10.1016/j.smim.2009.05.010; pmid: 19524453
29. F. Tzelepis *et al.*, Annexin1 regulates DC efferocytosis and cross-presentation during *Mycobacterium tuberculosis* infection. *J. Clin. Invest.* **125**, 752–768 (2015). doi: 10.1172/JCI77014; pmid: 25562320
30. Y. Zhang *et al.*, TTP-mediated regulation of mRNA stability in immune cells contributes to adaptive immunity, immune tolerance and clinical applications. *RNA Biol.* **18**, 2150–2156 (2021). doi: 10.1080/15476286.2021.1917185; pmid: 33866923
31. I. Dunand-Sauthier *et al.*, Silencing of c-Fos expression by microRNA-155 is critical for dendritic cell maturation and function. *Blood* **117**, 4490–4500 (2011). doi: 10.1182/blood-2010-09-308064; pmid: 21385848
32. J. G. Price *et al.*, CDKN1A regulates Langerhans cell survival and promotes Treg cell generation upon exposure to ionizing irradiation. *Nat. Immunol.* **16**, 1060–1068 (2015). doi: 10.1038/ni.3270; pmid: 26343536
33. D. F. Robbiani *et al.*, The leukotriene C(4) transporter MRP1 regulates CCL19 (MIP-3β, ELC)-dependent mobilization of dendritic cells to lymph nodes. *Cell* **103**, 757–768 (2000). doi: 10.1016/S0092-8674(00)00179-3; pmid: 11114332
34. N. Ali *et al.*, Skin-resident T cells drive dermal dendritic cell migration in response to tissue self-antigen. *J. Immunol.* **200**, 3100–3108 (2018). doi: 10.4049/jimmunol.1701206; pmid: 29563179
35. K. A. Hogquist *et al.*, T cell receptor antagonist peptides induce positive selection. *Cell* **76**, 17–27 (1994). doi: 10.1016/0092-8674(94)90169-4; pmid: 8287475

36. D. Xia, S. Hao, J. Xiang, CD8+ cytotoxic T-APC stimulate central memory CD8+ T cell responses via acquired peptide-MHC class I complexes and CD80 costimulation, and IL-2 secretion. *J. Immunol.* **177**, 2976–2984 (2006). doi: 10.4049/jimmunol.177.5.2976; pmid: 16920933
37. S. Chang-Rodriguez *et al*., Fetal and neonatal murine skin harbors Langerhans cell precursors. *J. Leukoc. Biol.* **77**, 352–360 (2005). doi: 10.1189/jlb.1004584; pmid: 15590753
38. G. Hoeffel *et al*., Adult Langerhans cells derive predominantly from embryonic fetal liver monocytes with a minor contribution of yolk sac-derived macrophages. *J. Exp. Med.* **209**, 1167–1181 (2012). doi: 10.1084/jem.20120340; pmid: 22565823
39. Y. Koyama, S. Nagao, K. Ohashi, H. Takahashi, T. Marunouchi, Sex differences in the densities of epidermal Langerhans cells of the mouse. *J. Invest. Dermatol.* **88**, 541–544 (1987). doi: 10.1111/1523-1747.ep12470104; pmid: 3572027
40. S. Joost *et al*., The molecular anatomy of mouse skin during hair growth and rest. *Cell Stem Cell* **26**, 441–457.e7 (2020). doi: 10.1016/j.stem.2020.01.012; pmid: 32109378
41. S. Joost *et al*., Single-cell transcriptomics reveals that differentiation and spatial signatures shape epidermal and hair follicle heterogeneity. *Cell Syst.* **3**, 221–237.e9 (2016). doi: 10.1016/j.cels.2016.08.010; pmid: 27641957
42. T. Jacob *et al*., Molecular and spatial design of early skin development, bioRxiv 522081 [Preprint] (2022); https://doi.org/10.1101/2022.12.28.522081.
43. S. Laffont *et al*., Androgen signaling negatively controls group 2 innate lymphoid cells. *J. Exp. Med.* **214**, 1581–1592 (2017). doi: 10.1084/jem.20161807; pmid: 28484078
44. E. Blanquart *et al*., Targeting androgen signaling in ILC2s protects from IL-33-driven lung inflammation, independently of KLRG1. *J. Allergy Clin. Immunol.* **149**, 237–251.e12 (2022). doi: 10.1016/j.jaci.2021.04.029; pmid: 33964300
45. T. Kobayashi *et al*., Homeostatic control of sebaceous glands by innate lymphoid cells regulates commensal bacteria equilibrium. *Cell* **176**, 982–997.e16 (2019). doi: 10.1016/j.cell.2018.12.031; pmid: 30712873
46. J. C. Nussbaum *et al*., Type 2 innate lymphoid cells control eosinophil homeostasis. *Nature* **502**, 245–248 (2013). doi: 10.1038/nature12526; pmid: 24037376
47. R. R. Ricardo-Gonzalez *et al*., Tissue signals imprint ILC2 identity with anticipatory function. *Nat. Immunol.* **19**, 1093–1099 (2018). doi: 10.1038/s41590-018-0201-4; pmid: 30201992
48. I. L. King, M. A. Kroenke, B. M. Segal, GM-CSF-dependent, CD103+ dermal dendritic cells play a critical role in Th effector cell differentiation after subcutaneous immunization. *J. Exp. Med.* **207**, 953–961 (2010). doi: 10.1084/jem.20091844; pmid: 20421390
49. M. Greter *et al*., GM-CSF controls nonlymphoid tissue dendritic cell homeostasis but is dispensable for the differentiation of inflammatory dendritic cells. *Immunity* **36**, 1031–1046 (2012). doi: 10.1016/j.immuni.2012.03.027; pmid: 22749353
50. A. Mortha *et al*., Microbiota-dependent crosstalk between macrophages and ILC3 promotes intestinal homeostasis. *Science* **343**, 1249288 (2014). doi: 10.1126/science.1249288; pmid: 24625929
51. C. Pearson *et al*., ILC3 GM-CSF production and mobilisation orchestrate acute intestinal inflammation. *eLife* **5**, e10066 (2016). doi: 10.7554/eLife.10066; pmid: 26780670
52. T. Castro-Dopico *et al*., GM-CSF calibrates macrophage defense and wound healing programs during intestinal infection and inflammation. *Cell Rep.* **32**, 107857 (2020). doi: 10.1016/j.celrep.2020.107857; pmid: 32640223
53. J. Mjösberg *et al*., The transcription factor GATA3 is essential for the function of human type 2 innate lymphoid cells. *Immunity* **37**, 649–659 (2012). doi: 10.1016/j.immuni.2012.08.015; pmid: 23063330
54. T. Sudo *et al*., Group 2 innate lymphoid cells support hematopoietic recovery under stress conditions. *J. Exp. Med.* **218**, e20200817 (2021). doi: 10.1084/jem.20200817; pmid: 33666647
55. Y. Simoni *et al*., Human innate lymphoid cell subsets possess tissue-type based heterogeneity in phenotype and frequency. *Immunity* **46**, 148–161 (2017). doi: 10.1016/j.immuni.2016.11.005; pmid: 27986455
56. N. Bechetoille *et al*., IL-13 is more efficient than IL-4 for recruiting Langerhans cell precursors from peripheral CD14+ monocytes. *Exogenous Dermatology* **1**, 279–289 (2002). doi: 10.1159/000069879
57. Y. Otsuka *et al*., Differentiation of Langerhans cells from monocytes and their specific function in inducing IL-22–specific Th cells. *J. Immunol.* **201**, 3006–3016 (2018). doi: 10.4049/jimmunol.1701402; pmid: 30322965
58. J.-Y. Cephus *et al*., Testosterone attenuates group 2 innate lymphoid cell-mediated airway inflammation. *Cell Rep.* **21**, 2487–2499 (2017). doi: 10.1016/j.celrep.2017.10.110; pmid: 29186686
59. G. Eberl, M. Colonna, J. P. Di Santo, A. N. McKenzie, Innate lymphoid cells. Innate lymphoid cells: A new paradigm in immunology. *Science* **348**, aaa6566 (2015). doi: 10.1126/science.aaa6566; pmid: 25999512
60. C. M. Lopes-Ramos, J. Quackenbush, D. L. DeMeo, Genome-wide sex and gender differences in cancer. *Front. Oncol.* **10**, 597788 (2020). doi: 10.3389/fonc.2020.597788; pmid: 33330090
61. W. Chen, D. Thiboutot, C. C. Zouboulis, Cutaneous androgen metabolism: Basic research and clinical perspectives. *J. Invest. Dermatol.* **119**, 992–1007 (2002). doi: 10.1046/j.1523-1747.2002.00613.x; pmid: 12445184
62. C. C. Zouboulis, The skin as an endocrine organ. *Dermatoendocrinol* **1**, 250–252 (2009). doi: 10.4161/derm.1.5.9499; pmid: 20808511
63. J. M. Ceruti, G. J. Leirós, M. E. Balañá, Androgens and androgen receptor action in skin and hair follicles. *Mol. Cell. Endocrinol.* **465**, 122–133 (2018). doi: 10.1016/j.mce.2017.09.009; pmid: 28912032
64. M. Li *et al*., Molecular signature and functional analysis of uterine ILCs in mouse pregnancy. *J. Reprod. Immunol.* **123**, 48–57 (2017). doi: 10.1016/j.jri.2017.09.003; pmid: 28915450
65. J. Siewiera *et al*., Circumvention of luteolysis reveals parturition pathways in mice dependent upon innate type 2 immunity. *Immunity* **56**, 606–619.e7 (2023). doi: 10.1016/j.immuni.2023.01.005; pmid: 36750100
66. M. Enamorado *et al*., Immunity to the microbiota promotes sensory neuron regeneration. *Cell* **186**, 607–620.e17 (2023). doi: 10.1016/j.cell.2022.12.037; pmid: 36640762
67. I. E. Adamopoulos, V. Kuchroo, IL-17A and IL-17F in tissue homeostasis, inflammation and regeneration. *Nat. Rev. Rheumatol.* **19**, 535–536 (2023). doi: 10.1038/s41584-023-01004-5; pmid: 37488297
68. J. Park *et al*., Shifts in the skin bacterial and fungal communities of healthy children transitioning through puberty. *J. Invest. Dermatol.* **142**, 212–219 (2022). doi: 10.1016/j.jid.2021.04.034; pmid: 34252398
69. T.-Y. Chuang, A. Popescu, W. P. D. Su, C. G. Chute, Basal cell carcinoma. A population-based incidence study in Rochester, Minnesota. *J. Am. Acad. Dermatol.* **22**, 413–417 (1990). doi: 10.1016/0190-9622(90)70056-N; pmid: 2312827
70. D. T. Gray *et al*., Trends in the population-based incidence of squamous cell carcinoma of the skin first diagnosed between 1984 and 1992. *Arch. Dermatol.* **133**, 735–740 (1997). doi: 10.1001/archderm.1997.03890420073008; pmid: 9197827
71. M. J. Castleman *et al*., Innate sex bias of *Staphylococcus aureus* skin infection is driven by α-hemolysin. *J. Immunol.* **200**, 657–668 (2018). doi: 10.4049/jimmunol.1700810; pmid: 29222165
72. B. L. Travi *et al*., Gender is a major determinant of the clinical evolution and immune response in hamsters infected with *Leishmania* spp. *Infect. Immun.* **70**, 2288–2296 (2002). doi: 10.1128/IAI.70.5.2288-2296.2002; pmid: 11953362
73. C. M. Lezama-Dávila, A. P. Isaac-Márquez, J. Barbi, S. Oghumu, A. R. Satoskar, 17β-estradiol increases Leishmania mexicana killing in macrophages from DBA/2 mice by enhancing production of nitric oxide but not pro-inflammatory cytokines. *Am. J. Trop. Med. Hyg.* **76**, 1125–1127 (2007). doi: 10.4269/ajtmh.2007.76.1125; pmid: 17556622
74. K. J. Bryson *et al*., BALB/c mice deficient in CD4 T cell IL-4Rα expression control Leishmania mexicana Load although female but not male mice develop a healer phenotype. *PLOS Negl. Trop. Dis.* **5**, e930 (2011). doi: 10.1371/journal.pntd.0000930; pmid: 21245915
75. L. K. Andersen, M. D. Davis, Sex differences in the incidence of skin and skin-related diseases in Olmsted County, Minnesota, United States, and a comparison with other rates published worldwide. *Int. J. Dermatol.* **55**, 939–955 (2016). doi: 10.1111/ijd.13285; pmid: 27009931
76. K. M. Uramoto *et al*., Trends in the incidence and mortality of systemic lupus erythematosus, 1950-1992. *Arthritis Rheum.* **42**, 46–50 (1999). doi: 10.1002/1529-0131(199901)42:1<46::AID-ANR6>3.0.CO;2-2; pmid: 9920013
77. S. R. Pillemer *et al*., Incidence of physician-diagnosed primary Sjögren syndrome in residents of Olmsted County, Minnesota. *Mayo Clin. Proc.* **76**, 593–599 (2001). doi: 10.1016/S0025-6196(11)62408-7; pmid: 11393497
78. C. Nannini, A. J. Jebakumar, C. S. Crowson, J. H. Ryu, E. L. Matteson, Primary Sjogren's syndrome 1976-2005 and associated interstitial lung disease: A population-based study of incidence and mortality. *BMJ Open* **3**, e003569 (2013). doi: 10.1136/bmjopen-2013-003569; pmid: 24282246
79. E. K. Johansson *et al*., Prevalence and characteristics of atopic dermatitis among young adult females and males-report from the Swedish population-based study BAMSE. *J. Eur. Acad. Dermatol. Venereol.* **36**, 698–704 (2022). doi: 10.1111/jdv.17929; pmid: 35032357
80. P. Mombaerts *et al*., RAG-1-deficient mice have no mature B and T lymphocytes. *Cell* **68**, 869–877 (1992). doi: 10.1016/0092-8674(92)90030-G; pmid: 1547488
81. J. Song *et al*., A mouse model for the human pathogen *Salmonella typhi*. *Cell Host Microbe* **8**, 369–376 (2010). doi: 10.1016/j.chom.2010.09.003; pmid: 20951970
82. J. Gschwend *et al*., Alveolar macrophages rely on GM-CSF from alveolar epithelial type 2 cells before and after birth. *J. Exp. Med.* **218**, e20210745 (2021). doi: 10.1084/jem.20210745; pmid: 34431978
83. C. Schneider *et al*., Frontline Science: Coincidental null mutation of Csf2rα in a colony of PI3Kγ-/- mice causes alveolar macrophage deficiency and fatal respiratory viral infection. *J. Leukoc. Biol.* **101**, 367–376 (2017). doi: 10.1189/jlb.4HI0316-157R; pmid: 27468760
84. C. Hurabielle *et al*., Immunity to commensal skin fungi promotes psoriasiform skin inflammation. *Proc. Natl. Acad. Sci. U.S.A.* **117**, 16465–16474 (2020). doi: 10.1073/pnas.2003022117; pmid: 32601220
85. A. I. Lim *et al*., Prenatal maternal infection promotes tissue-specific immunity and inflammation in offspring. *Science* **373**, eabf3002 (2021). doi: 10.1126/science.abf3002; pmid: 34446580
86. K. C. Valkenburg, S. R. Amend, K. J. Pienta, Murine prostate micro-dissection and surgical castration. *J. Vis. Exp.* **111**, e53984 (2016). pmid: 27213557
87. D. S. Lima-Junior *et al*., Endogenous retroviruses promote homeostatic and inflammatory responses to the microbiota. *Cell* **184**, 3794–3811.e19 (2021). doi: 10.1016/j.cell.2021.05.020; pmid: 34166614
88. M. I. Love, W. Huber, S. Anders, Moderated estimation of fold change and dispersion for RNA-seq data with DESeq2. *Genome Biol.* **15**, 550 (2014). doi: 10.1186/s13059-014-0550-8; pmid: 25516281
89. P. D. Thomas *et al*., PANTHER: Making genome-scale phylogenetics accessible to all. *Protein Sci.* **31**, 8–22 (2022). doi: 10.1002/pro.4218; pmid: 34717010
90. M. Stoeckius *et al*., Cell Hashing with barcoded antibodies enables multiplexing and doublet detection for single cell genomics. *Genome Biol.* **19**, 224 (2018). doi: 10.1186/s13059-018-1603-1; pmid: 30567574

ACKNOWLEDGMENTS

We thank C. Spinner and V. Lazarevic for providing Csf2$^{-/-}$ mice; T. Yoshida and J. H. Oh for maintaining and providing wildling mice and Red5 mice; K. L. Han, A. Terrell, S. Mistry, G. Koroleva, K. Beacht, E. Lewis, P. J. Perez-Chaparro, the NIAID animal facility, and the NIAID Microbiome Program gnotobiotic animal facility for technical support; M. Kasper, H. Yuan, M. Haniffa, and H. Gopee for data analysis support; A. Bendelac for providing help in this project; M. Smelkinson and O. Schwartz for assisting with the imaging assay; and all Belkaid laboratory members, especially P. Kulalert, T. Farley, and E. Ansaldo, for providing constructive feedback on this project and for critical reading of this manuscript. Schematic figures were created with BioRender (https://biorender.com). **Funding:** Y.B., L.C., I.G., D.C., S.J.H., V.M.L., C.A.R., A.C.W., N.C., N.B., are supported by the Division of Intramural Research of NIAID (NIAID; 1ZIA-AI001115 and 1ZIA-AI001132); L.C. is in part by the Office of Dietary Supplements Research Scholar program (NIH) and by the Cancer Research Institute Irvington Fellowship program; A.C.W. is in part by the Cancer Research Institute Irvington Fellowship program; A.I.L. is supported by the is supported by the Human Frontier Science Program (grant LT000191/2018); C.A.R. is the Lorraine W. Egan Fellow of the Damon Runyon Cancer Research Foundation (grant DRG-2496-23; and D.S.L.-J. in part by the Office of Dietary Supplements Research Scholar program (NIH) and the Pew Latin American Fellowship Program in the Biomedical Sciences from the Pew Charitable Trusts. B.R. is supported by the Intramural Research Program of NIDDK, NIH. C.S. is supported by the Swiss National Science Foundation (Eccellenza grant 194216) and the Peter Hans Hofschneider Professorship for Molecular Medicine The work in S.L. and J.C.-G. was supported by the Foundation pour la Recherche Medical (grant DEq. 20180339187 to JCG) and by the Agency National of Research (ANR-20-CE15-0027-01 to SL).
Author contributions: Conceptualization: Y.B., L.C., S.-J.H, A.I.L., N.C.; Investigation: L.C., C.L., I.G., J.G., D.C., S.-J.H., V.M.L., A.C.W.,

N.B., S.L., C.S.; Methodology: Y.B., L.C., S.-J.H, A.I.L., N.C., D.S.L.-J., M.E., C.A.R., B.R., J.-C.G., V.M.L., R.T., C.S.; Supervision: Y.B., S.-J.H, A.I.L., N.C., N.B.; Visualization: Y.B., L.C., N.B., C.L., I.G., J.G.; Writing – original draft: Y.B., L.C.; Writing – review and editing: Y.B., L.C., A.C.W. **Competing interests:** The authors declare no competing interests. **Data and materials availability:** *Csf2ra*$^{-/-}$ mice are available from M. Kopf under a material agreement with ETH Zürich. RNA-seq and scRNA-seq data were deposited into the Gene Expression Omnibus (GEO) data repository (GSE253295 for the whole study; GSE253293 for bulk RNA-seq of keratinocyte responses to *S. epidermidis*; and GSE253294 for scRNA-seq of DCs and T cell from the skin of males and females). All data needed to evaluate the conclusions are available in the main text or the supplementary materials.

SUPPLEMENTARY MATERIALS

science.org/doi/10.1126/science.adk6200
Figs. S1 to S5
Table S1
MDAR Reproducibility Checklist

Submitted 1 September 2023; accepted 26 February 2024
Published online 4 April 2024
10.1126/science.adk6200